The Astrophysical Journal, 652:994–1010, 2006 December 1
© 2006. The American Astronomical Society. All rights reserved. Printed in U.S.A.

SURVEY FOR GALAXIES ASSOCIATED WITH $z \sim 3$ DAMPED Lyα SYSTEMS. II. GALAXY-ABSORBER CORRELATION FUNCTIONS

Jeff Cooke[1,2] and Arthur M. Wolfe[1]
Department of Physics and Center for Astrophysics and Space Sciences, University of California, San Diego, Code 0424, La Jolla, CA 92093-0424; cooke@uci.edu, awolfe@ucsd.edu

Eric Gawiser[1,3]
Department of Astronomy, Yale University, P.O. Box 208101, New Haven, CT 06520-8101; gawiser@astro.yale.edu

and

Jason X. Prochaska[1]
University of California Observatories–Lick Observatory, University of California, Santa Cruz, CA 95064; xavier@ucolick.edu
Received 2006 March 21; accepted 2006 July 3

ABSTRACT

We use 211 galaxy spectra from our survey for Lyman break galaxies (LBGs) associated with 11 damped Lyα systems (DLAs) to measure the three-dimensional LBG autocorrelation and DLA-LBG cross-correlation functions with the primary goal of inferring the mass of DLAs at $z \sim 3$. From every measurement and test in this work, we find evidence for an overdensity of LBGs near DLAs that is very similar to that of LBGs near other LBGs. Conventional binning of the data while varying both r_0 and γ parameters of the fiducial model of the correlation function $\xi(r) = (r/r_0)^{-\gamma}$ resulted in the best-fit values and 1 σ uncertainties of $r_0 = 2.65 \pm 0.48$, $\gamma = 1.55 \pm 0.40$ for the LBG autocorrelation, and $r_0 = 3.32 \pm 1.25$, $\gamma = 1.74 \pm 0.36$ for the DLA-LBG cross-correlation function. To circumvent shortcomings found in binning small data sets, we perform a maximum likelihood analysis based on Poisson statistics. The best-fit values and 1 σ confidence levels were found to be $r_0 = 2.91^{+1.0}_{-1.0}$, $\gamma = 1.21^{+0.6}_{-0.3}$ for the LBG autocorrelation, and $r_0 = 2.81^{+1.4}_{-2.0}$, $\gamma = 2.11^{+1.3}_{-1.4}$ for the DLA-LBG cross-correlation function. We report a redshift spike of five LBGs with $\Delta z = 0.015$ of the $z = 2.936$ DLA in the PSS 0808+5215 field; the DLA-LBG clustering signal survives when omitting this field from the analysis. Using the correlation function measurements and uncertainties, we compute the $z \sim 3$ LBG galaxy bias $b_{\rm LBG}$ to be $1.5 < b_{\rm LBG} < 3$, corresponding to an average halo mass of $10^{9.7} < \langle M_{\rm LBG} \rangle < 10^{11.6}\ M_\odot$, and the $z \sim 3$ DLA galaxy bias $b_{\rm DLA}$ to be $1.3 < b_{\rm DLA} < 4$, corresponding to an average halo mass of $10^9 < \langle M_{\rm LBG} \rangle < 10^{12}\ M_\odot$. Finally, two of the six QSOs discovered were found to lie within $\Delta z = 0.0125$ of two of the survey DLAs. We estimate that the probability of this occurring by chance is 1 in 940, indicating a possible relationship between the distribution of QSOs and DLAs at $z \sim 3$.

Subject headings: galaxies: formation — galaxies: high-redshift — quasars: absorption lines

Online material: color figures

1. INTRODUCTION

One of the most fundamental measurements of high-redshift galaxies is their spatial distribution, largely because this information can be used to infer their average dark matter halo mass. Standard cold dark matter (CDM) cosmology details the process by which galaxies formed by the gravitational collapse of primordial dark matter density fluctuations. In the early universe, low-mass fluctuations typically had density contrasts high enough to collapse against the Hubble flow and formed uniformly throughout space, whereas high-mass fluctuations with high-density contrasts were rare. However, the superposition of density fluctuations resulted in the collapse of an excess number of high-mass fluctuations clustered near the peaks of underlying mass overdensities that sufficiently enhanced their density contrast. It is in this context that the measurement of the clustering of galaxies infers the underlying dark matter halo mass of these systems.

Several surveys over the last decade have been used to infer the dark matter mass of high-redshift galaxy populations by their angular clustering (e.g., Daddi et al. 2000, 2004; McCarthy et al. 2001, 2004; Porciani & Giavalisco 2002; Foucaud et al. 2003). One population, the LBGs, are identified photometrically by the decrement (break) in their continua shortward of the Lyman limit caused by absorption from optically thick intervening systems in the line of sight. The spectroscopic survey of Steidel et al. (1998) provided sufficient spectra for a measurement of the three-dimensional distribution of LBGs at $z \sim 3$. Analysis of that data by Adelberger et al. (1998) showed evidence of significant clustering, corresponding to halo masses of $\sim 10^{11}$–$10^{12} M_\odot$. The faint emission from LBGs restricts observations to low signal-to-noise ratio, low-resolution spectra using current technology. As a consequence, the properties of this magnitude-limited sample must be examined statistically and/or from composite spectra. In addition, the selection methods employed to detect LBGs are not sensitive to all types of galaxies at high redshift and are therefore partially incomplete.

Quasar absorption-line systems provide a complementary means to study high-redshift systems. Their detection is dependent only on the brightness of the background source and the strength of the absorption-line features and is not biased by intrinsic magnitudes or photometric selection criteria. DLAs are defined to have

[1] Visiting Astronomer, W. M. Keck Telescope. The Keck Observatory is a joint facility of the University of California, the California Institute of Technology, and NASA, and was made possible by the generous financial support of the W. M. Keck Foundation.

[2] Current address: Center for Cosmology, University of California, Irvine, CA 92697.

[3] NSF Astronomy and Astrophysics Postdoctoral Fellow.

TABLE 1
SURVEY FIELDS

Field	R.A. (J2000.0)	Decl. (J2000.0)	z_{QSO}	$z_{DLA(s)}$	log N(H I)	log N(H I) Refs.	$E(B-V)$
LBQS 0056+0125	00 59 17.62	+01 42 05.30	3.149	2.775	21.0	1	0.03
PKS 0336−017	03 39 00.65	−01 33 19.20	3.197	3.062	21.2	2	0.14
PSS 0808+5215	08 08 49.43	+52 15 14.90	4.450	2.936, 3.113	20.9, 20.7	3; 4	0.04
PSS 0957+3308	09 57 44.50	+33 08 23.00	4.250	3.280	20.5	4	0.01
BRI 1013+0035	10 15 48.96	+00 20 19.52	4.381	3.103	21.1	5	0.03
PSS 1057+4555	10 57 56.39	+45 55 51.97	4.116	3.050, 3.317	20.3, 20.3	5, 6; 7	0.01
PSS 1432+3940	14 32 24.90	+39 40 24.00	4.280	3.272	21.3	4	0.01
PC 1643+4631A	16 45 01.09	+46 26 16.44	3.790	3.137	20.7	8	0.02
JVAS 2344+3433	23 44 51.25	+34 33 48.64	3.053	2.908	21.1	4	0.08

NOTE.—Units of right ascension are hours, minutes, and seconds, and units of declination are degrees, arcminutes, and arcseconds.
REFERENCES.—(1) Wolfe et al. 1995; (2) Prochaska et al. 2001; (3) Paper 1; (4) Prochaska et al. 2003; (5) Storrie-Lombardi & Wolfe 2000; (6) Péroux et al. 2001; (7) Lu et al. 1998; (8) Schneider et al. 1991.

column densities of $N(\mathrm{H\ I}) > 2 \times 10^{20}$ atoms cm^{-1} (Wolfe et al. 1986, 2005) and contain ~80% of the H I content of the universe (Prochaska et al. 2005). Systems with such high column densities provide self-shielding against the ambient ionizing radiation and thereby protect large reservoirs of neutral gas. Several lines of evidence, including high-resolution analysis of DLA gas kinematics (Prochaska & Wolfe 1997, 1998; Wolfe & Prochaska 2000a, 2000b) and the agreement between the comoving neutral gas density at $z > 2$ and the mass density of visible stars in local disks (Wolfe et al. 1995), have fueled the belief that DLAs are capable of evolving into present-day galaxies like the Milky Way (Kauffmann 1996).

It becomes clear that studies of galaxy formation are incomplete without understanding the population of protogalaxies that DLAs represent. Although properties such as the gas kinematics and chemical abundances of DLAs can be studied with high resolution and are well documented, the mass of these systems has remained unknown. The sparse distribution of DLAs in quasi-stellar object (QSO) sight lines prohibits the use of their clustering as a tracer of the underlying dark matter mass. Instead, the host halo mass of DLAs can be inferred by their cross-correlation with another known population. In this work, we use the ubiquitous LBGs at $z \sim 3$ for this purpose. This paper is the second in a series (Cooke et al. 2005, hereafter Paper I) reporting the results of a survey of LBGs detected near 11 DLAs at $z \sim 3$, with the primary goal of inferring the mass of DLAs from the DLA-LBG spatial cross-correlation.

This paper is organized as follows. We briefly review the imaging and spectroscopic observations in § 2 and present spectra of the objects detected near the DLAs in § 3 and the spectra of the faint active galactic nucleus (AGN) discovered in the survey in § 4. We describe the methodology behind the clustering analysis in § 5 and present the LBG autocorrelation and DLA-LBG cross-correlation results by technique, including tests of these results, in § 6. We discuss the implications on the galaxy bias and mass of DLAs in § 7 and provide a brief discussion in § 8 and a summary of the survey in § 9. We adopt $\Omega_M = 0.3, \Omega_\Lambda = 0.7, h = 100$ cosmology unless otherwise noted, primarily for direct comparison to the literature. All correlation lengths r_0 reported in this work are in h^{-1} Mpc comoving.

2. SURVEY DESIGN

Our first goal was to efficiently select LBGs at $z \sim 3$ via their photometric colors. To achieve this, we developed a $u'BVRI$ photometric selection technique, primarily due to filter availability, that fulfilled the imaging goals and resulted in an efficacy very similar to previous work. Our second observational goal was the accurate acquisition and analysis of a few hundred faint $z \sim 3$ galaxy spectra. This was accomplished using the Keck telescope and low-resolution multiobject spectroscopy. A detailed description of the data acquisition, reduction and analysis, and comparison to previous $U_nG\mathcal{R}I$ surveys can be found in Paper I. Here, we discuss a few relevant points of the observations.

2.1. *The DLA Sample*

The QSO fields targeted in this survey were selected from the subset that met the following constraints: (1) The QSO was required to display at least one known DLA in the redshift range where our $u'BVRI$ photometric selection is most effective ($2.6 < z < 3.4$), (2) systems within 3000 km s^{-1} from the background QSO were not used to avoid proximity effects, and (3) a preference was given to fields that would be observed through the lowest airmass and in the direction of lowest Galactic reddening to minimize the flux attenuation of $z \sim 3$ sources. Table 1 lists our survey fields. At the time this survey began, only ~30 DLAs met these criteria. From this subset, the targets were chosen at random. The mean column density of the 11 DLAs in this survey is $\log N(\mathrm{H\ I}) = 20.94$ atoms cm^{-2}, with a typical individual error of ±0.1, whereas the mean DLA column density measured recently from 197 DLAs taken over the same redshift range from the Sloan Digital Sky Survey (SDSS; Prochaska et al. 2005) is $N(\mathrm{H\ I}) = 20.84$ atoms cm^{-2} and a typical error of ±0.2. Therefore, the DLAs presented here appear to be a good representation of $z \sim 3$ DLAs, on average.

2.2. *Imaging*

We obtained deep $u'BVRI$ imaging of nine QSO fields with 11 known $z \sim 3$ DLAs from 2000 April to 2003 November using the Low Resolution Imager and Spectrometer (LRIS; Oke et al. 1995) on the 10 m Keck I telescope, and the Carnegie Observatories Spectrograph and Multiobject Imaging Camera (COSMIC; Kells et al. 1998) on the 5 m Hale telescope at the Palomar Observatory. Object placement and image field size are topics that deserve a brief discussion. The DLAs were approximately centered in the images, in which seven have a field of view of $\sim 6' \times 7.'5$ (LRIS) and two have a field of view $\sim 9.'7 \times 9.'7$ (COSMIC). The usable area of each of the final stacked images was reduced in both dimensions by $\lesssim 40''$ from our imposed dithering sequence. This resulted in maximum (diagonal) comoving object separations of $\sim 10\ h^{-1}$ Mpc (LRIS) and $\sim 13\ h^{-1}$ Mpc (COSMIC) at $z \sim 3$ and about half this distance for the DLAs. The correlation length of LBGs at $z \sim 3$ has been measured to be $3.96 \pm 0.29\ h^{-1}$ Mpc by Adelberger et al. (2003, hereafter A03). As a result, the angular clustering component in our survey cannot be measured much beyond

1–2 correlation lengths, yet the redshift path of $\sim 540\ h^{-1}$ Mpc, where our photometric selection is best described ($2.6 < z < 3.4$), allows complete analysis of the distribution of the LBGs in the redshift direction.

2.2.1. *Photometric Color Selection*

We searched for star-forming galaxies at $z \sim 3$ with expectations and spectral profiles described in previous work (Steidel et al. 1996a, 1996b; Lowenthal et al. 1997; Pettini et al. 2000; Shapley et al. 2003). The $u'BVRI$ filters are well suited to select these objects via their broadband colors. It is important to note that surveys with these expectations, although efficient in detecting a large number of galaxies at $z \sim 3$, are not sensitive to all galaxies that may exist at high redshift and the corresponding underlying dark matter they may trace. For example, systems with excessive intrinsic extinction or older stellar populations will not be selected. In our effort to mimic previous surveys, we remain partially incomplete to all galaxies at $z \sim 3$, but include a significant number to provide meaningful statistics toward the goal of cross-correlating LBGs with DLAs. From the complete list of sources detected in each field, we selected LBG candidates that met the following color constraints,

$$(u' - B)_{\rm AB} > 1.1 \quad (1)$$

$$(u' - V)_{\rm AB} > 1.6 \quad (2)$$

$$0.6 < (B - R)_{\rm AB} < 2.1 \quad (3)$$

$$(V - R)_{\rm AB} < 0.6 \quad (4)$$

$$(V - I)_{\rm AB} < 0.6 \quad (5)$$

$$20.0 < R_{\rm AB} < 25.5, \quad (6)$$

and assigned these candidates the highest priority. Some candidates were selected using a subset of these constraints and assigned a lower priority. An additional set of candidates was selected by relaxing equations (1)–(6) by 0.2 mag and was assigned the lower respective priority. This was done in an effort to include objects that would be overlooked due to photometric errors arising from statistical and systematic uncertainties. All LBG candidates were then slated by priority for follow-up spectroscopy.

2.3. *Spectroscopy*

Spectroscopic observations were obtained from 2000 November through 2004 February using LRIS on the Keck I telescope. Spectra were acquired using either the 300 line $\rm mm^{-1}$ grating on the red arm, the 300 line $\rm mm^{-1}$ grism on the blue arm, or both. We used multiobject slit masks with $1''.0-1''.5$ slitlets, chosen according to the seeing conditions whenever possible, providing a spectral resolution of 9–12 Å FWHM. We obtained spectroscopy of 529 LBG color candidates that resulted in 339 redshift identifications, largely a consequence of weather, instrument failures, and shortened exposure times. We conservatively identified 211 $z > 2$ LBGs for use in the analyses in this work. Details regarding the efficiency of the $u'BVRI$ photometric selection and the subsequent redshift identifications can be found in Paper I. In short, low-resolution, low signal-to-noise ratio spectra of this caliber result in redshift identifications that vary in confidence. The efficiency of identified $z > 2$ objects that met the photometric criteria was as low as 62% for stringent identifications and as high as 95% when including the low-confidence identifications. The redshift distribution of $z > 2$ LBGs used in the analysis is shown in Figure 1.

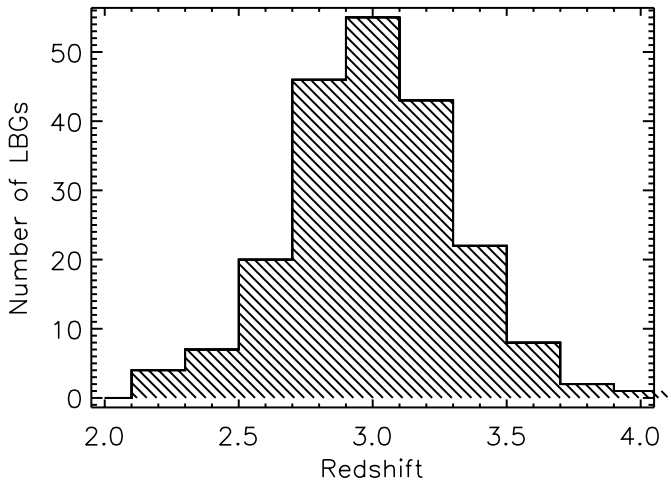


FIG. 1.—Redshift distribution of the $z > 2$ objects detected in this survey, binned with $\Delta z = 0.2$. The $u'BVRI$ color selection technique results in a Gaussian distribution of spectroscopically confirmed objects centered at $z = 3.02 \pm 0.32$.

2.3.1. *LBG Redshifts*

LBGs have prominent rest-frame UV spectral features from 912 to ~1700 Å (Pettini et al. 2000; Shapley et al. 2003) that are redshifted to ~3200–7500 Å for objects at $z \sim 3$. These features are identifiable in spectra with moderate to low signal-to-noise ratios. All LBGs in this work were identified following the procedure described in Paper I. Redshifts were determined using Lyα features, continuum profiles, and one-to-many stellar and interstellar absorption and emission lines. The observed discrepancy between the Lyα emission and interstellar absorption redshifts witnessed to some extent in all LBG spectra to date is attributed to the effects of galactic-scale stellar and supernovae-driven winds. The uncertainty in systemic redshift caused by this discrepancy was minimized by adopting the corrections outlined in A03 and presented below. These corrections were formulated from the results of rest-frame optical nebular measurements of a sample of LBGs (Pettini et al. 2001), with the justification that the gas responsible for LBG nebular lines [O II] λ3727, Hβ, and [O III] $\lambda\lambda$4959, 5007 closely traces the redshifts of the stellar populations.

For LBGs displaying Lyα in emission, the correction to the systemic redshift velocity determined solely from the observed Lyα emission feature is

$$v_{{\rm Ly}\alpha} \simeq +670 - 8.9 W_\lambda\ {\rm \AA}^{-1}\ {\rm km\ s^{-1}}, \quad (7)$$

where W_λ is the rest-frame equivalent width of the Lyα emission in Å. In cases where the redshift is determined by the Lyα feature and the equivalent width is uncertain, the correction is

$$v_{{\rm Ly}\alpha} \simeq +310\ {\rm km\ s^{-1}}. \quad (8)$$

For LBGs displaying Lyα and interstellar metal absorption lines, the mean velocity is corrected by

$$v_{\rm abs} \simeq -0.114\Delta v + 230\ {\rm km\ s^{-1}}, \quad (9)$$

where Δv is the velocity difference between the Lyα feature and the average of the interstellar absorption lines. Finally, the velocity correction

$$v_{\rm abs} \simeq -150\ {\rm km\ s^{-1}} \quad (10)$$

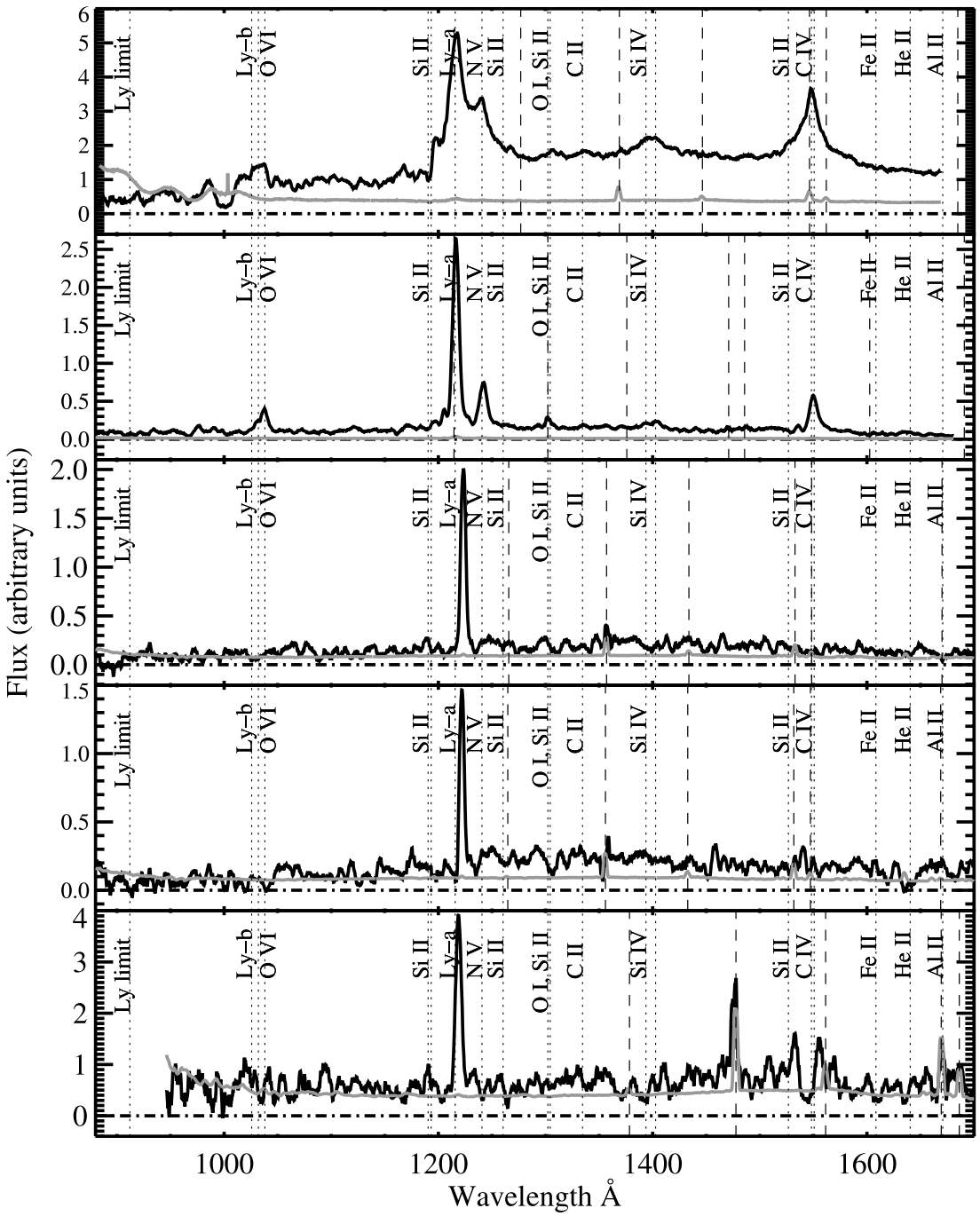


FIG. 2.— Individual spectra of the 13 LBGs and 2 QSOs that reside within $\Delta z = 0.0125$ of the 11 DLAs. In addition, we include the spectra of two LBGs found within $\Delta z = 0.015$ of the $z = 2.936$ DLA in the PSS 0808+5215 field. Error arrays are overlaid (in gray), and expected interstellar and stellar absorption lines are indicated using vertical dotted lines. Bright night-sky emission lines, which can be difficult to subtract completely in fainter spectra, are marked with vertical dashed lines. These spectra range from the lowest to highest signal-to-noise ratio of the complete sample. They are smoothed by 15 pixels for clarity over the wavelength range shown and to help highlight the break(s) in the continua; however, the sharpness of the individual emission and absorption lines is affected. *Top to bottom*: Objects 0336−0782 (QSO found near the DLA in the PKS 0336−017 field), 0957−0859 (QSO found near the DLA in the PSS 1057+4555 field), 1013−0210, 1013−0661, and 0056−0993. [*See the electronic edition of the Journal for a color version of this figure.*]

is applied to the redshifts determined solely by the average of the measured interstellar absorption lines.

These formulae are expected to diminish the redshift uncertainties caused by galactic outflows to within an rms scatter of $\sim$200 km s^{-1} ($\Delta z \sim 0.002$ at $z \sim 3$). No correction was made for the unknown peculiar velocities of the LBGs. We used as much information as possible from our set of 211 $z > 2$ LBGs and nearly always secured more than one absorption line for each LBG spectrum (see Paper I). We found a negligible effect on the resulting correlation functions when using equations (8) and (10) compared to using equations (7) and (9).

3. SPECTRA OF SYSTEMS NEAR DLAs

Figures 2–4 present the individual spectra of the 15 systems (13 LBGs and 2 QSOs) within $\Delta z = 0.0125$ of the 11 DLAs in this survey. In addition, we have included the spectra of two LBGs

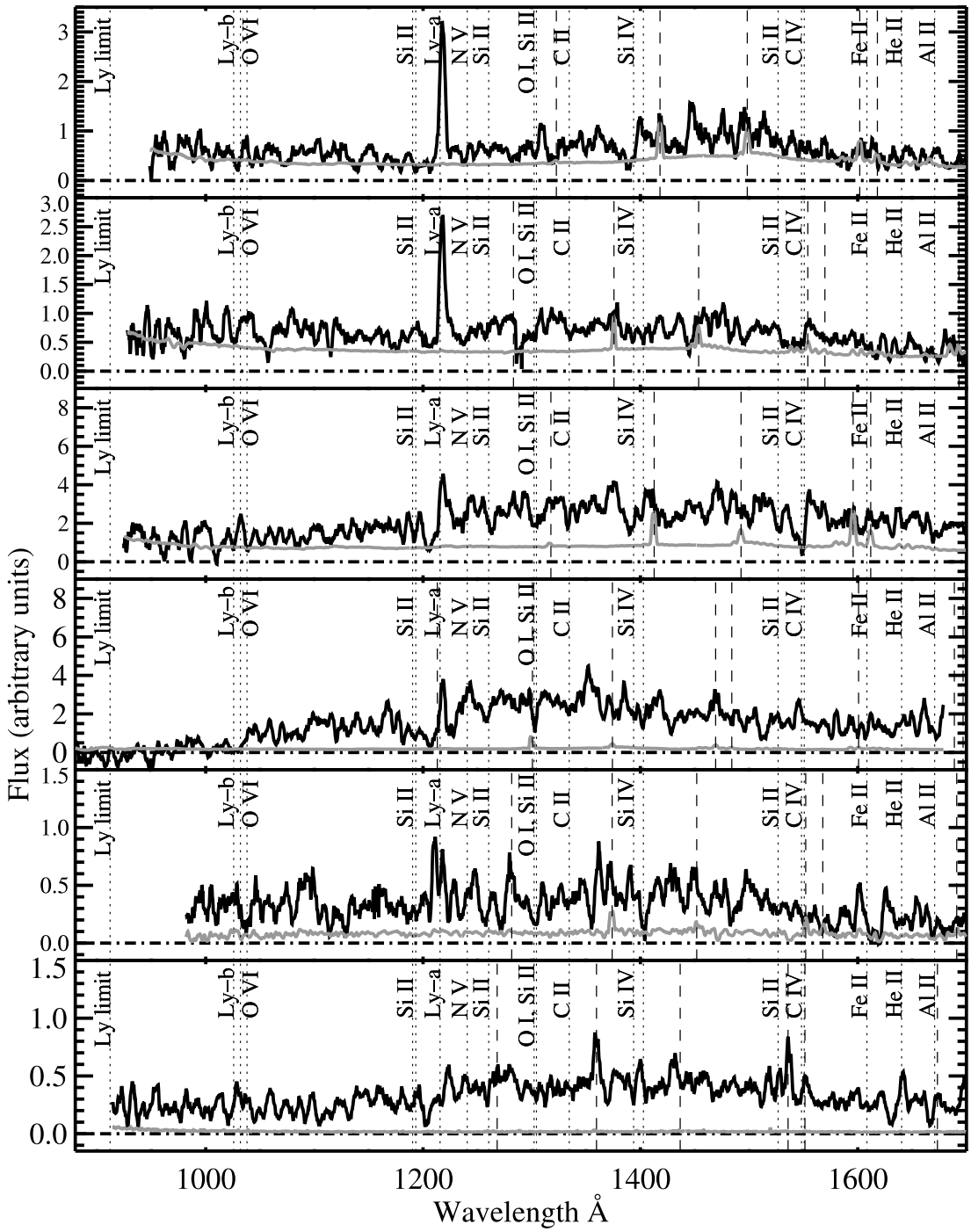


FIG. 3.—Same as Fig. 2. *Top to bottom*: Objects 0808−0944, 1057−1278, 0808−0377, 0957−1284, 0808−0506, and 0336−0758. [*See the electronic edition of the Journal for a color version of this figure.*]

found within $\Delta z = 0.015$ of the $z = 2.936$ DLA in the PSS 0808+5215 field (see § 6.3.2). The low signal-to-noise ratio spectra have been smoothed by 15 pixels. This large smoothing allows the coarse features of the continua to be seen more readily on the wavelength scales presented here, but diminishes the appearance of individual absorption features. These range from the highest to the lowest signal-to-noise ratio spectra in the complete sample. As presented in Paper I, these spectra are best referenced to, and studied as, composite spectra of galaxies displaying similar spectral profiles.

In nearly all spectra, a decrement in the continuum is visible shortward of 1216 Å caused by absorption from optically thick intervening systems at lower redshift (the Lyα forest). LBGs are faint sky-dominated objects, and bright night-sky emission lines can be difficult to subtract cleanly from the spectra. Therefore, the positions of the sky emission lines are marked to prevent the misidentification of residual sky flux as real LBG features. No order-blocking filter was used in these observations, resulting in an underestimation of the flux longward of ~6300 Å in the observation frame or longward of ~1500 Å in the rest frame.

Overall, the spectra of the systems near DLAs appear to be those of typical LBGs, and we find a similar ratio of emission-identified LBGs to absorption-identified LBGs as in the complete sample. Excluding QSOs, the 15 LBGs presented here exhibit a magnitude

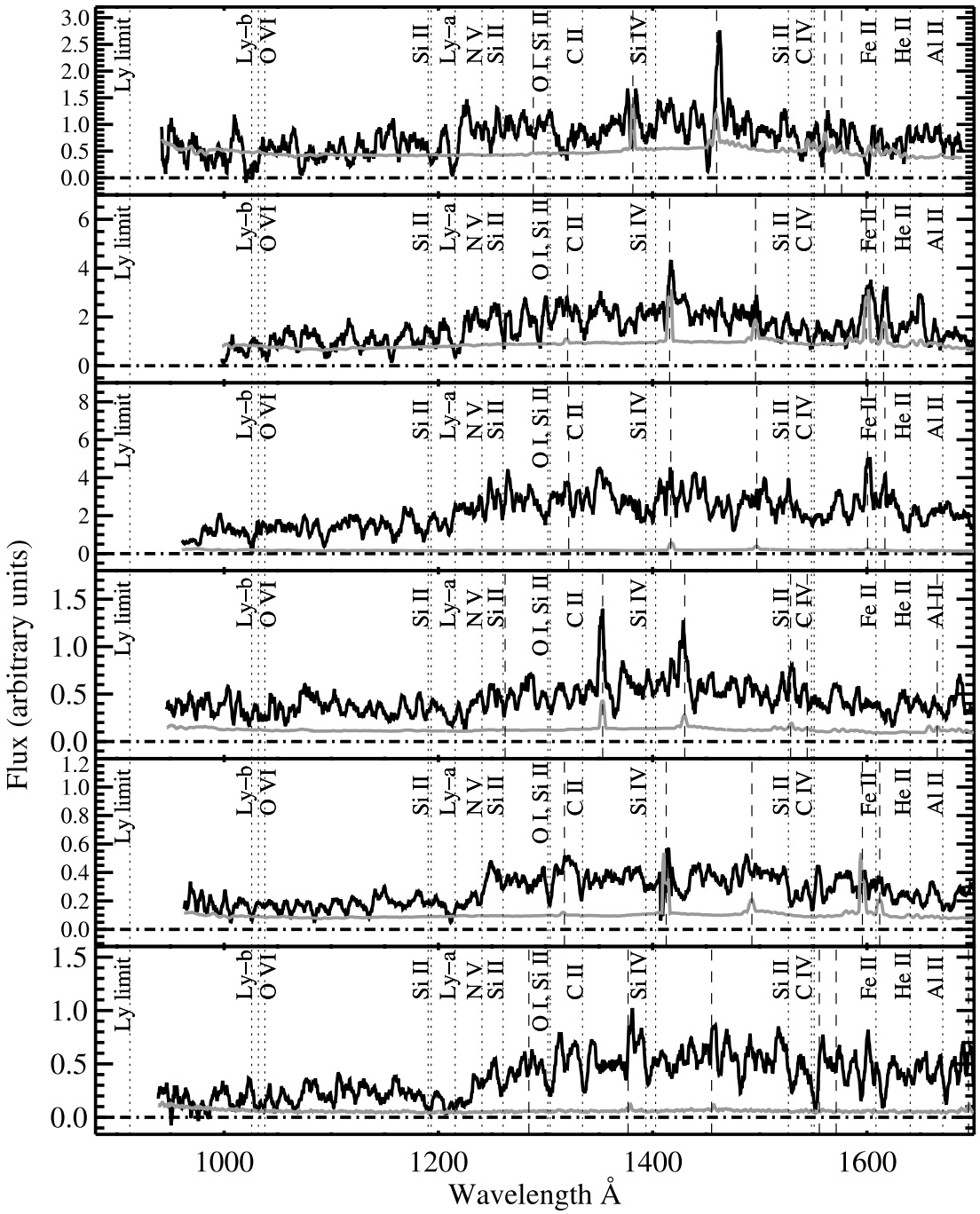


FIG. 4.—Same as Fig. 2. *Top to bottom*: Objects 1057−3646, 0808−1264, 0808−0269, 0808−0556, 0808−1801, and 1057−0600. [*See the electronic edition of the Journal for a color version of this figure.*]

range of $23.1 < R < 25.4$. The set of 205 LBGs with no apparent AGN activity has a magnitude range of $22.1 < R < 25.5$, where $R = 25.5$ is the practical spectroscopic magnitude limit of Keck using the LRIS instrument. The R-magnitude distribution of these objects against the full set of LBGs is shown in Figure 5. A two-sided Kolmogorov-Smirnov test resulted in a value of 0.6 and a high probability that the cumulative distribution functions of both data sets are significantly similar.

4. FAINT AGNs

Figure 6 presents the smoothed spectra of six Lyman break objects displaying AGN activity discovered in the 465 arcmin^2 of this survey. These six $20.1 < R < 24.4$ objects are separate and distinct from the nine QSOs targeted in this survey and result in a faint AGN number density of $\sim$46 deg^{-2}. Three objects are broad-line AGNs with FWHM > 2000 km s^{-1} and display several broad emission features that are typical of QSOs, and the remaining three display emission lines with FWHM < 2000 km s^{-1}, including Lyα and at least one other high-ionization species indicative of a hard spectrum. The spectrum of object 0808−0876 did not extend to C IV $\lambda\lambda$1548, 1551, but detailed inspection does show O VI $\lambda\lambda$1032, 1038, N V λ1240, and possible S IV $\lambda\lambda$1394, 1402 emission. As a result, this object cannot be ruled out as an LBG in the conventional sense of the term.

It is interesting to note that two of the six QSOs were discovered within $\Delta r_z = 0.0125$ ($<10\ h^{-1}$ Mpc) of two DLAs. Object

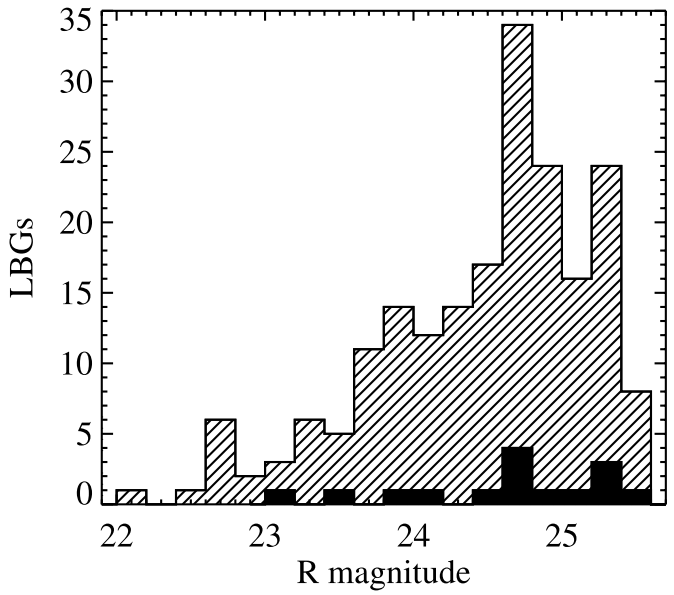


FIG. 5.—Histogram of the R-magnitude distribution of the full $2.6 < z < 3.4$ LBG sample (*hatched*) and the LBGs near DLAs (*filled*). A two-sided Kolmogorov-Smirnov test revealed a high probability that the two cumulative distribution functions are significantly similar.

0957−0859, an $R = 23.3$ narrow-line QSO at $z = 3.283$, lies near the $z = 3.279$ DLA in the PSS 0957+3308 field at an angular separation of $241''$. Object 0336−0782 at $z = 3.074$ is a brighter, $R = 20.1$ broad-line QSO and lies at an angular separation of $167''$ from the $z = 3.062$ DLA in the PKS 0336−017 field. Since the appearance of two QSOs at small separations from the two DLAs seemed unlikely, we tested this in the following manner. We assumed the detection of one QSO per survey DLA field (we found six QSOs in nine fields) and ran a Monte Carlo simulation of 10,000 realizations corrected by the photometric selection function. From this, we estimate a 3.8% and 2.8% chance that a QSO would reside randomly within $\Delta r_z = 0.0125$ of the $z = 3.062$ and $z = 3.279$ DLA, respectively. More importantly, we estimate 1 chance in 940 that a QSO would reside within $\Delta r_z = 0.0125$ of *both* DLAs. This is significant to $\sim 4\ \sigma$ and may have important implications on the distribution of QSOs with DLAs. The close proximity of the QSOs with the DLAs may provide insight into the duty cycle of QSOs and the overall size and survival of high-column-density neutral gas reservoirs in environments with sources of significant ionizing flux. More research into this relationship is necessary and is one of the goals of our ongoing One-Degree Deep (ODD) survey (J. Cooke et al. 2006, in preparation).

In subsequent sections, we focus on the distribution of the LBG population as a whole. Throughout, we search for evidence of an overdensity of LBGs near DLAs over random and compare this to the overdensity of LBGs near other LBGs. We describe the approach adopted to estimate the three-dimensional LBG autocorrelation and DLA-LBG cross-correlation functions and present several techniques to measure and test these functions from the data set.

5. CORRELATION FUNCTIONS: METHODOLOGY

For a random distribution of LBGs, the joint probability of finding an LBG occupying volume element dV_1 and another LBG occupying volume element dV_2 at a separation r is (Peebles 1980)

$$dP(r) = \bar{n}^2_{\rm LBG}\, dV_1\, dV_2, \tag{11}$$

where $\bar{n}_{\rm LBG}$ is the mean density of LBGs averaged over the realization. In general, for any given distribution of LBGs, this expression becomes

$$dP(r) = \bar{n}^2_{\rm LBG}[1 + \xi_{\rm LBG}(r)]\, dV_1\, dV_2, \tag{12}$$

where $\xi_{\rm LBG}(r)$ is the LBG autocorrelation function. In this context, $\xi_{\rm LBG}(r)$ quantifies the excess probability over random.

Similarly, for two populations (here DLAs and LBGs), the joint probability of finding an object from the first population at a distance r from an object of the second population is

$$dP(r) = \bar{n}_{\rm DLA}\bar{n}_{\rm LBG}[1 + \xi_{\rm DLA\text{-}LBG}(r)]\, dV_{\rm DLA}\, dV_{\rm LBG}, \tag{13}$$

where $\bar{n}_{\rm DLA}$ is the mean density of DLAs, and $\xi_{\rm DLA\text{-}LBG}(r)$ is the cross-correlation function also quantifying the excess probability over random. From this, the conditional probability of finding an LBG at a distance r from a known DLA is

$$dP(r) = \bar{n}_{\rm LBG}[1 + \xi_{\rm DLA\text{-}LBG}(r)]\, dV_{\rm LBG}. \tag{14}$$

Based on studies of nearby galaxies, it has been commonly assumed that $\xi(r)$ follows a power law of the form

$$\xi(r) = \left(\frac{r}{r_0}\right)^{-\gamma}. \tag{15}$$

This has been a reasonable assumption given that the power spectrum is well fit by a power law and that $\xi(r)$ is essentially the Fourier transform of the power spectrum. In this form, the parameters r_0 and γ are all that are needed to describe the correlation function. In practice, $\xi(r)$ is estimated by comparing the galaxy separations found in the data to the galaxy separations in mock catalogs of randomly distributed galaxies. These random galaxy catalogs mimic the angular and spatial configuration of the data (e.g., Davis & Peebles 1983; Hawkins et al. 2003; A03). By carefully restricting the random galaxy catalogs to the exact constraints of the real data, complications caused by edge effects, bright objects, and the physical constraints of the instruments are removed or well constrained.

5.1. *Spatial Correlation Estimator*

There have been several methods proposed and used to estimate $\xi(r)$ from galaxy catalogs. We adopt the method of Landy & Szalay (1993), which is well suited for small galaxy samples and has the least bias present in commonly used estimators (Kerscher et al. 2000). This technique involves comparing the number of galaxy pairs in the data having separations within a given spatial interval $r \pm \delta r$ to the number of galaxy pairs in the random galaxy catalogs having separations within the same spatial interval. To reduce shot noise, the random galaxy catalogs are made many times ($\sim$100 times) larger than the data sample and normalized to the data. The number of pairs is counted in each spatial bin determined in logarithmic or linear space. From the normalized bin counts, the LBG autocorrelation function $\xi_{\rm LBG\text{-}LBG}(r)$ is estimated as

$$\xi_{\rm LBG\text{-}LBG}(r) = \frac{D_{\rm LBG}D_{\rm LBG} - 2D_{\rm LBG}R_{\rm LBG} + R_{\rm LBG}R_{\rm LBG}}{R_{\rm LBG}R_{\rm LBG}}, \tag{16}$$

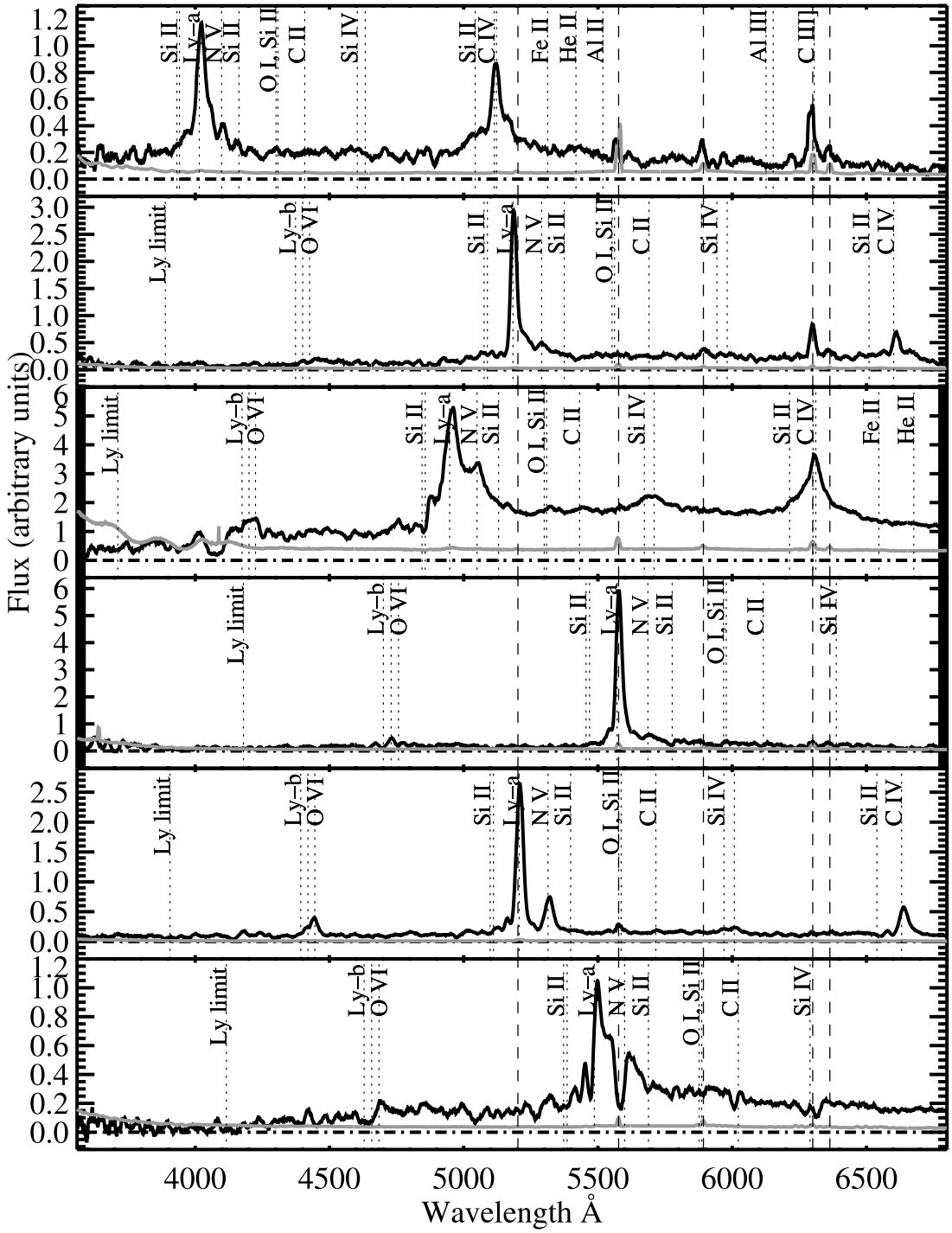


FIG. 6.—Spectra of the six $20.0 < R < 25.5$ QSOs discovered in this survey, with the error arrays overlaid (in gray). Some identified emission and absorption lines are marked with vertical dotted lines and labeled. Bright night-sky emission lines are marked with vertical dashed lines. Night-sky lines can be difficult to subtract completely in the fainter spectra. *Top to bottom*: Objects 0056−1085, 0336−0645, 0336−0782, 0808−0876, 0957−0859, and 1057−3225. [*See the electronic edition of the Journal for a color version of this figure.*]

and the DLA-LBG cross-correlation function $\xi_{\mathrm{DLA\text{-}LBG}}(r)$ is estimated as

$$\xi_{\mathrm{DLA\text{-}LBG}}(r) = \frac{D_{\mathrm{DLA}}D_{\mathrm{LBG}} - D_{\mathrm{DLA}}R_{\mathrm{LBG}} - R_{\mathrm{DLA}}D_{\mathrm{LBG}} + R_{\mathrm{DLA}}R_{\mathrm{LBG}}}{R_{\mathrm{DLA}}R_{\mathrm{LBG}}}, \quad (17)$$

where the separations between galaxies in the data constitute the *DD* catalogs, separations between random galaxies make up the *RR* catalogs, and separations between data and random galaxies make up the *DR* and *RD* cross-reference catalogs. Equations (16) and (17) are identically used to estimate the projected angular correlation functions ω_p in § 6.1.

6. CORRELATION FUNCTIONS: RESULTS BY TECHNIQUE

We present several approaches to measure and test for an overdensity of LBGs near LBGs, and LBGs near DLAs over random.

We first describe the correlation functions as determined by a conventional binning technique. We find a dependence of the correlation function on bin parameters and circumvent this shortcoming, which can be pronounced for small data sets by performing a maximum likelihood analysis and comparing the results. The maximum likelihood method makes the most of the data set and is a direct and essentially bin-independent way to determine the clustering behavior. Finally, we test the effects that the physical constraints of the slit masks and the presence of an individual overdense field have on the correlation function. The redshift separations in all analyses were determined in a consistent manner.

6.1. *Conventional Binning*

We followed the modification to conventional radial bins suggested by A03 in an effort to diminish the effects that the LBG redshift uncertainties caused by galactic-scale winds have on the clustering amplitude. In doing so, we also provide a means for direct comparison by methodology of our measure of the LBG autocorrelation and the DLA-LBG cross-correlation functions to the LBG autocorrelation function of A03. In this treatment, the number of pairs that reside in concentric "cylindrical" bins with dimensions $r_\theta \pm \delta r_\theta$ and $r_z \pm \delta r_z$ is counted. Limits are placed on r_z such that it is the greater of $7r_\theta$ and 1000 km s$^{-1}(1+z)/H(z)$ and chosen to be several times larger than the redshift uncertainties. Here we interpreted $(1+z)$ as $(1+\bar{z})$, where $\bar{z}$ is the average redshift of the two objects. The length in redshift of each bin is fixed ($\sim 9\ h^{-1}$ Mpc at $z \sim 3$) for small r_θ and grows as $7r_\theta$ when r_θ becomes large. The lower limit is placed to avoid missing correlated pairs, and the upper limit reaches down the correlation function to include >80% of the correlated pairs for $\gamma \gtrsim 1.6$.

We measured out to the maximum angular separation of $\theta = 300''$ and used logarithmic $r_\theta \pm dr_\theta$ bins to remain consistent with the parameters chosen by A03. Recalling that the fields in this survey are $\sim 6' \times 7.'5$, the number of pairs with separations at larger radii diminishes rapidly. Assuming the canonical power-law form of the correlation function (eq. [15]), the expected excess number of pairs using this approach is

$$\omega_p(r_\theta, < r_z) \equiv \frac{\langle n \rangle}{\bar{n}} - 1 = \frac{r_0^\gamma r_\theta^{1-\gamma}}{2r_z} B\left(\frac{1}{2}, \frac{\gamma-1}{2}\right) I_x\left(\frac{1}{2}, \frac{\gamma-1}{2}\right), \tag{18}$$

where $\langle n \rangle$ is the expected number of objects, $\bar{n}$ is the number of objects in a random sight line, and B and I_x are the beta and incomplete beta functions with $x \equiv r_z^2(r_z^2 + r_\theta^2)^{-1}$ (see § 6.4 of Press et al. 1992). The best-fit values of r_0 and γ of the correlation function result from fitting equation (18) to the observed number of pairs measured by the above binning scheme. The fundamental errors in ω_p are dependent on our choice of estimator. Using the estimators in equations (16) and (17), the errors $\delta\omega_p(\theta)$ are described by (Roche et al. 1999; Foucaud et al. 2003)

$$\delta\omega_p(\theta) = \sqrt{\frac{1+\omega_p(\theta)}{DD}}, \tag{19}$$

where DD represents either the $D_{\rm LBG}D_{\rm LBG}$ or $D_{\rm DLA}D_{\rm LBG}$ pair catalogs.

The uncertainties of the functional fits were estimated by running a Monte Carlo simulation of the measured correlation function. As described in Appendix C of A03, this approach is to create a large number (we performed 1000) of realizations of ω_p by adding a Gaussian deviate to the fundamental error and minimizing the χ^2 fit. The range of 68% of the best-fit parameter values is what we report as the best-fit value 1 σ uncertainty when using this method. These uncertainties may be underestimated by a factor of 1–2, as argued in Adelberger et al. (2005) and Adelberger (2005).

6.1.1. *LBG Autocorrelation*

A03 reported the values and 1 σ uncertainties of $r_0 = 3.96 \pm 0.29$ and $\gamma = 1.55 \pm 0.15$ for the LBG autocorrelation at $z \sim 3$. As stated above, we fit our data in an identical manner as A03, including the Monte Carlo error analysis. The best-fit values and 1 σ uncertainties for our data set are $r_0 = 2.65 \pm 0.48$ and $\gamma = 1.55 \pm 0.40$ and are shown in Figure 7, with the published results of A03 overlaid for comparison. The bin errors shown in the figure (and all subsequent figures by this method) are the error estimates on ω_p using equation (19). We find a possibly weaker clustering amplitude for $z \sim 3$ LBGs in our sample, as compared to A03, yet consider the possible error underestimation on the functional fit to the data as mentioned above. In addition, subtleties involved in random catalog generation, sample variance and sample size, estimation of the $U_nG\mathcal{R}I$ versus $u'BVRI$ photometric selection function profiles, LBG redshift assignments, and our inability to accurately measure the correlation function at separations smaller than $\sim 0.5\ h^{-1}$ Mpc may contribute as well. In the remaining plots, all comparisons of the best-fit values for the LBG autocorrelation and the DLA-LBG cross-correlation must consider these possible differences.

6.1.2. *DLA-LBG Cross-correlation*

We performed the above binning technique on the cross-catalogs of DLA and LBG separations to determine the first spectroscopic measure of the DLA-LBG cross-correlation function. The best fit to the cross-correlation data resulted in values and 1 σ uncertainties of $r_0 = 3.32 \pm 1.25$ and $\gamma = 1.74 \pm 0.36$ (Cooke et al. 2006) and is shown in Figure 7. Upon inspection, it is immediately apparent that the DLA-LBG cross-correlation function has a slope and correlation length similar to the LBG autocorrelation function. The angular range of the plot (~ 0.4–$3\ h^{-1}$ Mpc) reflects the limits on the correlation measurement caused by placing the DLAs in the center of our images. Although the uncertainty in either cross-correlation parameter is large, the measured central values indicate an overdensity of LBGs near DLAs to 1–2 σ.

6.1.3. *Inclusion of Previous Work*

The data from the four DLAs in the survey of Steidel et al. (2003, hereafter S03), and the 11 DLAs from this work, constitute the largest available spectroscopic sample of DLAs and LBGs to measure the spatial DLA-LBG cross-correlation function. The similarity in techniques and instruments used in both surveys allowed a direct combination of the data once the few differences were addressed and corrected to the best of our abilities. We used the available online data set[4] of S03 but note that because of this, our knowledge in some areas of their observations was limited. In lieu of Lyα equivalent width information for each LBG in their sample, we were restricted to using equations (8) and (10) to determine the systemic redshifts of 880 LBGs in 17 fields (and later a subsample of 700 in 15 fields from K. L. Adelberger [2004, private communication]). The area of each S03 field was estimated by the extent of the angular positions of their spectroscopic data (this assumes a position angle identical to, or having a right angle to, P.A. = 0 for each slit mask). Random catalogs were

[4] Files obtained from http://vizier.cfa.harvard.edu/viz-bin/VizieR?-source=J/ApJ/592/728/.

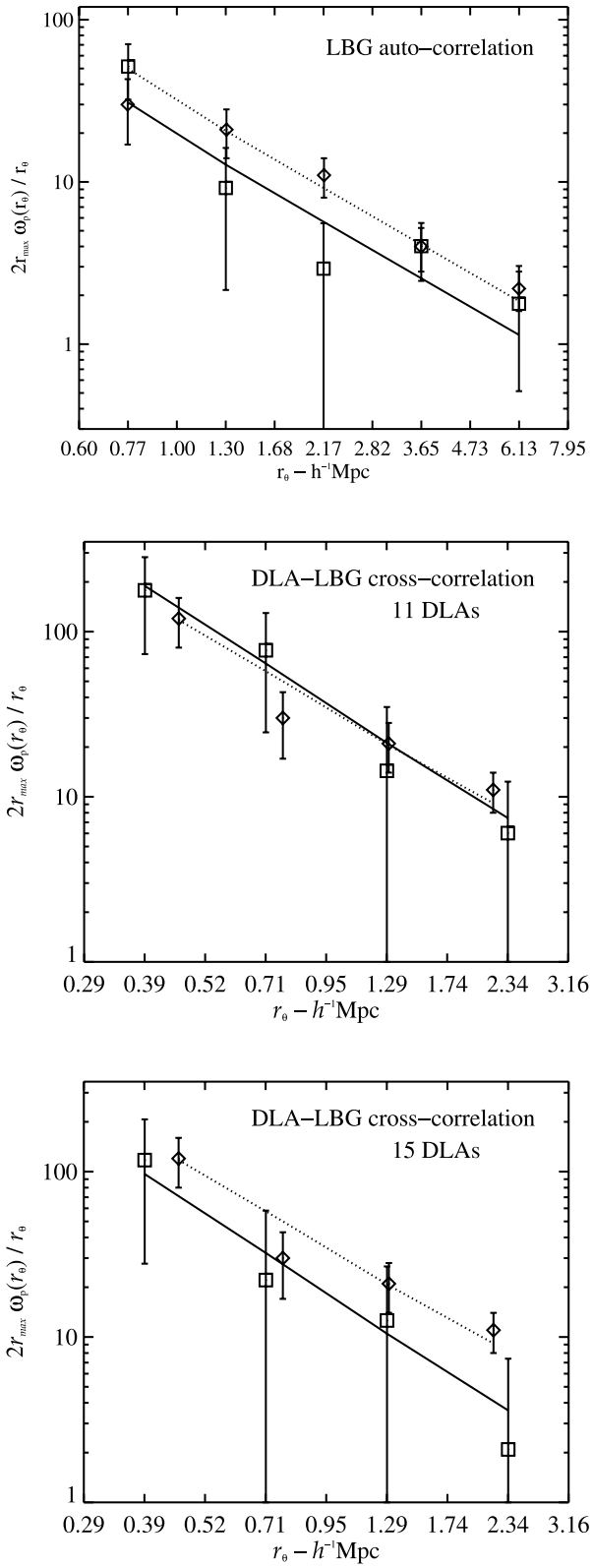


FIG. 7.—Plot of the LBG autocorrelation and DLA-LBG cross-correlation functions, using the binning technique described in the text. The correlation functions are shown as squares and best fit as the solid lines. We measure the best-fit values and $1\,\sigma$ errors of $r_0 = 2.65 \pm 0.48$, $\gamma = 1.55 \pm 0.40$ for the LBG autocorrelation (*top panel*); $r_0 = 3.32 \pm 1.25$, $\gamma = 1.74 \pm 0.36$ for the DLA-LBG cross-correlation of the 11 DLAs in this survey (*middle panel*); and $r_0 = 2.70 \pm 1.16$, $\gamma = 1.73 \pm 0.39$ for the DLA-LBG cross-correlation of the combined set of 15 DLAs (*bottom panel*) that includes four DLAs from the survey of S03. The errors shown are those determined by eq. (19). Overlaid in diamonds are the data for the LBG autocorrelation from A03 and best fit to that data, marked by the dotted lines, for comparison. [*See the electronic edition of the Journal for a color version of this figure.*]

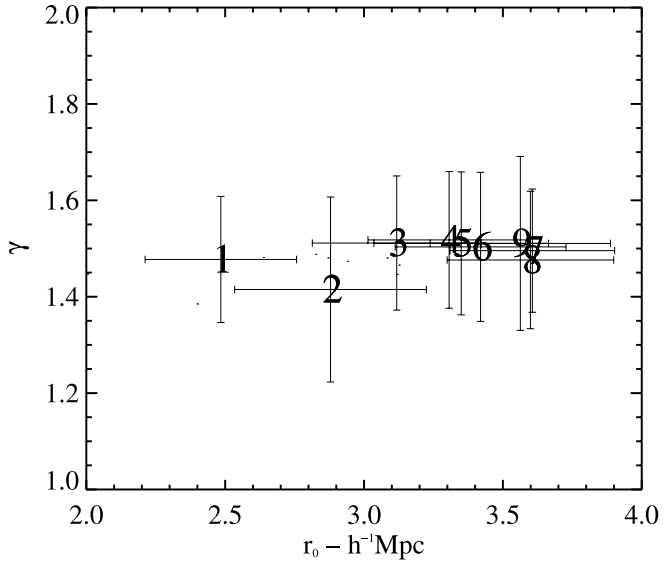


FIG. 8.—Scatter plot of the LBG autocorrelation from our analysis of the data set of S03. We measured the parameters while varying the logarithmic bin size from 1.125 to 0.225 (labeled 1–9) over a fixed interval of $r_\theta \sim 0.04$–$8\ h^{-1}$ Mpc. The effect of bin size on the correlation values is readily apparent. Although the values appear to converge, smaller samples only allow a few larger bins and may not converge.

generated in the same manner as described above, using these field sizes and the observed density of their sample.

Once we were satisfied with our duplication of the LBG autocorrelation of A03, we measured the best-fit values and $1\,\sigma$ uncertainties of $r_0 = 2.20 \pm 0.96, \gamma = 1.77 \pm 0.40$ for the DLA-LBG cross-correlation for the full set of 15 DLAs. The results are presented in Figure 7. It can be seen that evidence for an overdensity of LBGs near DLAs survives and, acknowledging the above caveats and our efforts to correct the differences between the two surveys, the 15 DLAs may provide a better sample to determine the cross-correlation parameters of DLAs at $z \sim 3$.

6.2. *Maximum Likelihood*

Arbitrary binning of the data into coarse bins introduces uncertainties because the value of $\xi(r)$ can depend on the bin size, interval, and bin center. Dependence on bin size is illustrated in Figure 8. In that plot, we varied the bin size from logarithmic intervals of 0.225 to 1.125 over a fixed $r_\theta \sim 0.04$–$8\ h^{-1}$ Mpc and found that r_0 varied from $\sim$2.0 to 3.1 h^{-1} Mpc and that γ varied from $\sim$1.35 to 1.48 in our analysis of the S03 sample. To remedy this problem, we estimated the value of r_0 and γ in the most direct way possible. We maximized the likelihood that a power law of the form $\xi(r) = (r/r_0)^{-\gamma}$ would produce the observed pair separations (Croft et al. 1997; Mullis et al. 2004).

Poisson probabilities are valid in the limit where the number of bins is large and the probability per bin is small. Constructing bin separations on such a fine level as to include either 1 or 0 LBGs per bin allows us to form the likelihood function. The probabilities associated with the bins are assumed independent of each other in the sparse sampling limit. The probability P of finding ν_i observed pairs, where μ_i pairs are expected, is the Poisson probability

$$P_{\mu_i}(\nu_i) = \frac{e^{-\mu_i}\mu_i^{\nu_i}}{\nu_i!}. \tag{20}$$

The likelihood function $\mathcal{L}$ is the product of the probability of having exactly one pair in every interval where one pair exists

in the data and exactly zero in all others and is defined in terms of the joint probabilities,

$$\mathcal{L} = \prod_{i}^{N} \frac{e^{-\mu_i}\mu_i^{\nu_i}}{\nu_i!} \prod_{j\neq i}^{N} \frac{e^{-\mu_j}\mu_j^{\nu_j}}{\nu_j!}, \tag{21}$$

where μ_i is the expected number of pairs in the interval dr, ν_i is the observed number of pairs for that same interval, and the index j runs over the elements where there are no pairs. This can also be expressed as

$$\ln \mathcal{L} = \sum_{i}^{N} (-\mu_i + \nu_i \ln \mu_i - \ln \nu_i!) + \sum_{j\neq i}^{N} \left(-\mu_j + \nu_j \ln \mu_j - \ln \nu_j!\right). \tag{22}$$

The expected number of objects μ_i for a given radial separation is obtained by solving equations (16) and (17) for $D_{\rm LBG}D_{\rm LBG}$ and $D_{\rm DLA}D_{\rm LBG}$, respectively. As stated above, we used the assumption that $\xi(r) = (r/r_0)^{-\gamma}$ (eq. [15]) and varied the values of both r_0 and γ to determine the values of maximum likelihood. The maximum likelihood was determined by minimizing the conventional expression

$$S = -2 \ln \mathcal{L} \tag{23}$$

and using $\Delta S = S(r_{\rm best}, \gamma_{\rm best}) - S(r_0, \gamma)$ to determine χ^2 confidence levels, observing that the values of S had χ^2 distributions.

The maximum likelihood technique is a powerful tool in measuring the likelihood of a given functional fit to the data but has at least one shortcoming in the form presented here. As mentioned above, the Poisson approximation is valid in the regime large interval number (very small separation radius) and low probability. But, even large random catalogs will occasionally find zero pairs in the very small intervals where this approximation is most accurate. In these cases, the likelihood may be less accurate or undefined. Therefore, we imposed the following two conditions (C. R. Mullis 2005, private communication): (1) the number of separations in the data-random cross-catalogs *DR* (and *RD*) must be greater than zero for each bin, which indirectly imposes the same condition on the random-random catalogs *RR* since they are larger; and (2) imposing the constraint that $[\xi(r) - 1] > 2DR/RR$ {or $[\xi(r) - 1] > (DR + RD)/RR$ for the cross-correlation}. For the few values of r where these criteria were not met, the expected value of *DD* was interpolated across the finely spaced intervals. Interpolating the few instances where this occurred had little impact on the final result because there were far fewer of these intervals when compared to the total used for analysis.

6.2.1. *LBG Autocorrelation*

The maximum likelihood values for the LBG autocorrelation and 1 σ confidence levels were found to be $r_0 = 2.91^{+1.0}_{-1.0}$ and $\gamma = 1.21^{+0.6}_{-0.3}$. The probability contours are shown in the top panel of Figure 9, where, in addition, we overlay both the maximum likelihood value and 1 σ confidence level of r_0 for a fixed $\gamma = 1.6$, and the best-fit values and 1 σ errors of the LBG autocorrelation function of A03, for comparison. The values of r_0 and γ determined by this method are consistent to within their errors with those found using conventional binning. Moreover, the maximum likelihood technique yields the same results regardless of the number intervals tested.

6.2.2. *DLA-LBG Cross-correlation*

Since the maximum likelihood method is well suited for small samples, we readily applied it toward the DLA-LBG

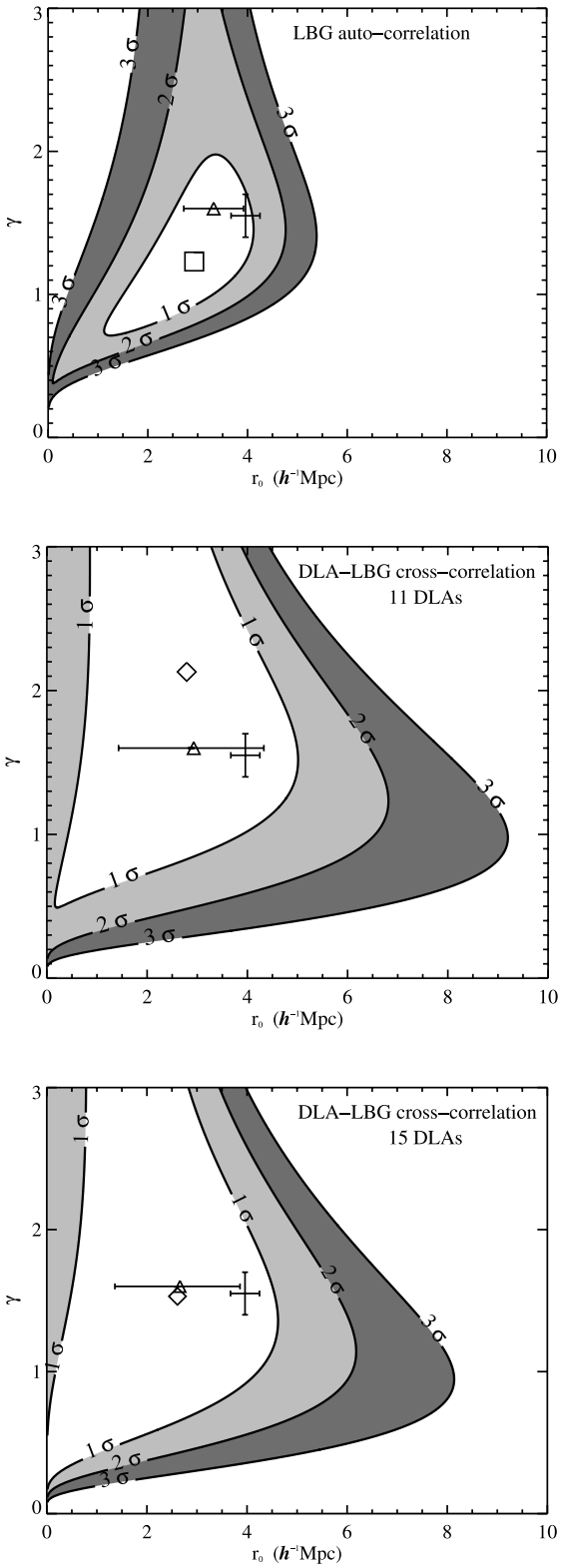


FIG. 9.— Correlation function probability contours for two free parameters, as measured by the maximum likelihood method. *Top*: The square at $r_0 = 2.91$, $\gamma = 1.21$ marks the maximum likelihood values for the LBG autocorrelation for our survey. *Middle*: The diamond marks the maximum likelihood values of $r_0 = 2.81$ and $\gamma = 2.11$ for the DLA-LBG cross-correlation. *Bottom*: The diamond marks the maximum likelihood values $r_0 = 2.66$ and $\gamma = 1.59$ for the DLA-LBG cross-correlation for the combined sample of 11 DLAs from this survey and the four DLAs from the survey of S03. The triangles on each plot, and 1 σ error bars, are the best-fit values (one free parameter) of r_0 for a fixed value of $\gamma = 1.6$. The error crosses indicate the values and 1 σ errors for the LBG autocorrelation, as determined byA03. The 1, 2, and 3 σ confidence regions are labeled. [*See the electronic edition of the Journal for a color version of this figure.*]

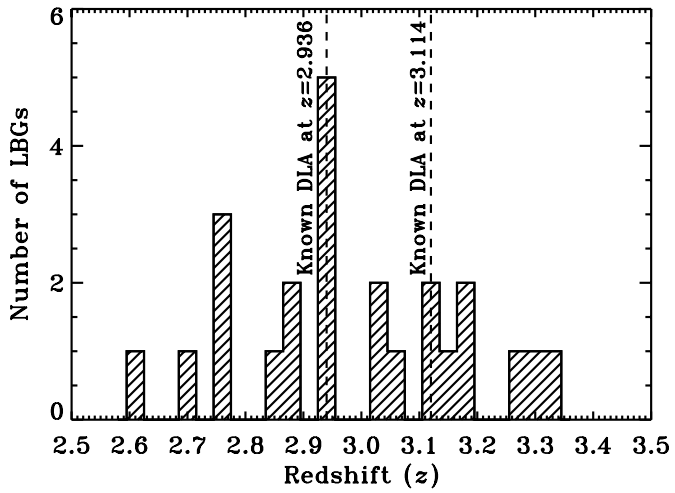


FIG. 10.—Redshift histogram of the $2.6 < z < 3.4$ LBGs in the PSS 0808+5215 field. Objects are binned with $\Delta z = 0.03$. The redshifts of the two known DLAs are indicated by the vertical dashed lines.

TABLE 2
PSS 0808+5215 CELL COUNTS

r_z	h^{-1} Mpc[a]	LBGs[b]
0.0025	1.68	2
0.0050	3.36	2
0.0075	5.03	3
0.0100	6.71	3
0.0125	8.38	3
0.0150	10.05	5
⋮	⋮	5
0.0450	29.99	6

[a] $\Omega_M = 0.3$, $\Omega_\Lambda = 0.7$.
[b] Number of LBGs found in cells with dimensions $\sim 5'.5 \times 7'$ ($\sim 7 \times 10\ h^{-2}$ Mpc^2 at $z = 3$) and $2r_z$, centered on the $z = 2.936$ DLA. Typical errors in LBG redshifts caused by galactic-scale winds are $\sim 2\ h^{-1}$ Mpc.

cross-correlation measurement. The analysis found maximum likelihood values and 1 σ confidence levels of $r_0 = 2.81^{+1.4}_{-2.0}$ and $\gamma = 2.11^{+1.3}_{-1.4}$ for the set of 11 DLAs and $r_0 = 2.66^{+1.9}_{-2.1}$ and $\gamma = 1.59^{+1.6}_{-0.9}$ for the full set of 15 DLAs, with the probability contours shown in Figure 9 (*middle and bottom panels, respectively*). We found that 65%–90% of the maximum likelihood values indicate a nonzero r_0, depending on the value of γ. Although the uncertainties are large, the best-fit values using the maximum likelihood technique also suggest an overdensity of LBGs near DLAs with 1–2 σ confidence, similar to the results using conventional binning.

6.3. *Tests*

This survey uses the distribution of LBGs determined from multiobject spectroscopic data to measure the correlation functions. Here we test the contributions to the correlation functions by the physical constraints of the multiobject slit masks and test the strength of the clustering signal in the absence of the DLA having the largest overdensity of LBGs.

6.3.1. *Physical Constraints of the Observations*

A false enhancement of the clustering signal can occur when the finite number of multiobject slit masks do not cover the full area of the imaged fields. This effect can be problematic in every survey and is nearly removed here by the fact that seven out of the nine fields were imaged with the relatively small field of view LRIS camera and have spectroscopic coverage over their entire area. The remaining two fields, imaged by the larger-field-of-view COSMIC, have $\sim$70% areal spectroscopic coverage. However, any augmentation to the correlation functions from these two fields was virtually eliminated by confining our random catalogs to the precise areas sampled by the slit masks and by the fact that these two fields have few spectra and make a small contribution to the final results.

Perhaps a more prominent effect is the dilution to the clustering signal from the fact that only a finite number of objects is allowed on each slit mask. All but one of the LBG candidates that lie in conflict in the dispersion direction are compromised. Similarly, LBGs that cluster tightly in angular space require many slit masks for proper spectroscopic coverage, which is not usually feasible. In order to minimize this, we observed two to three overlapping slit masks in most fields. Even so, there remain a few tightly clustered LBG candidates, as well as LBG candidates that were in conflict in the dispersion direction that have no spectral coverage to date. To measure the extent to which this physical constraint affects the clustering signal, we compared the results of the correlation functions using random catalogs having galaxies with the exact angular positions of the data to those using random catalogs having galaxies with random angular positions.

The correlation measurements presented in §§ 6.1 and 6.2 used random galaxy catalogs having the exact angular positions of the data. We remeasured the correlation functions using these techniques, but allowed the galaxies in the random catalogs to have random angular positions. Doing so, we found the best-fit parameters and 1 σ uncertainties for the LBG autocorrelation to be $r_0 = 2.31 \pm 0.55$, $\gamma = 1.47 \pm 0.40$ for the conventional binning method, and $r_0 = 2.08^{+1.0}_{-1.1}$, $\gamma = 1.49^{+1.1}_{-0.5}$ for the maximum likelihood method. Duplicating this for the DLA-LBG cross-correlation of the 11 DLAs in our survey (and the combined set of 15 DLAs), we found the best-fit parameters and 1 σ uncertainties to be $r_0 = 3.21 \pm 0.95$, $\gamma = 2.03 \pm 0.22$ ($r_0 = 2.52 \pm 0.92$, $\gamma = 1.71 \pm 0.46$) using conventional binning, and $r_0 = 3.20^{+2.2}_{-2.9}$, $\gamma = 1.62^{+1.4}_{-1.0}$ ($r_0 = 2.44^{+1.3}_{-1.9}$, $\gamma = 2.41^{-1.6}_{-1.7}$) using the maximum likelihood technique. There was no apparent trend in either parameter, which suggests that the physical constraints of the slit masks had a weak effect on our survey as a whole. This was suspected, since, in most cases, we obtained overlapping spectroscopic coverage. Although the central values of the parameters are increased in some cases and decreased in others, they are within error in all cases.

6.3.2. *The PSS 0808+5215 Field*

Field-by-field analysis revealed a relative spike of five LBGs with $\Delta z < 0.015$ ($<10\ h^{-1}$ Mpc) to the $z = 2.936$ DLA in the PSS 0808+5215 field. A redshift histogram of the $2.6 < z < 3.4$ LBGs in the PSS 0808+5215 field is shown in Figure 10. To estimate the probability of this overdensity occurring by chance, we ran 10,000 random simulations of the distribution of the $2.6 < z < 3.4$ LBGs detected in the field corrected by the photometric selection function. We found five LBGs within $\Delta z = 0.015$ of the $z = 2.936$ DLA 0.16% of the time. Therefore, we conclude that this is most likely a real overdensity. To illustrate the extent of the overdensity, Table 2 lists the number of LBGs in cells centered on the $z = 2.936$ DLA with varying radius in redshift. We find the next nearest LBG at $\Delta z = 0.043$, or 29.9 h^{-1} Mpc.

Inspection of the angular distribution of the LBGs in the two-dimensional image indicates that we may not be seeing the full extent of the overdensity because of the relatively small field of

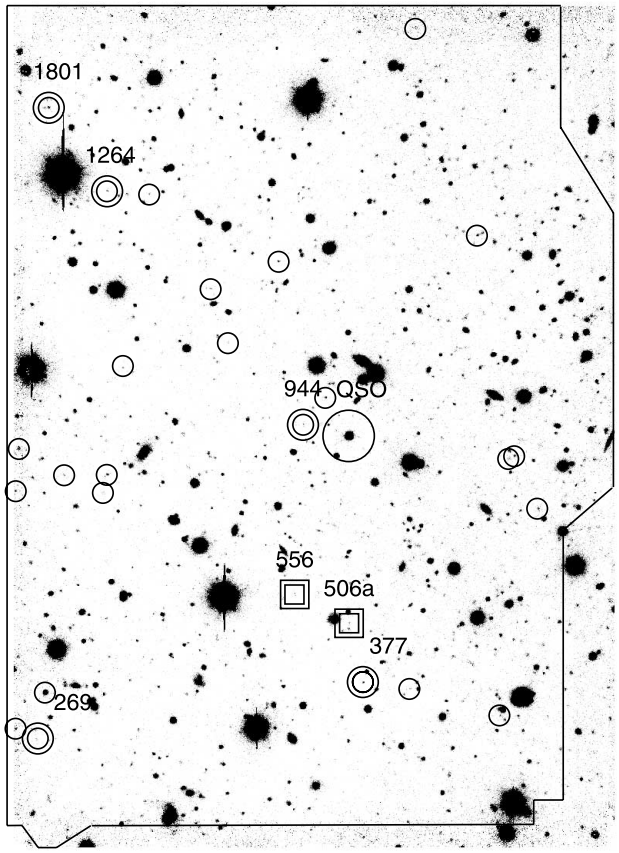


FIG. 11.—*R*-band image of LBGs identified in the PSS 0808+5215 field. The central $z = 4.45$ QSO displays DLAs at $z = 2.936$ and 3.114. The QSO is indicated by the large circle. The five LBGs associated with the $z = 2.936$ DLA are shown using two concentric circles, and the two LBGs associated with the $z = 3.114$ DLA are shown using two concentric squares. All other spectroscopically confirmed LBGs are shown as small (*black*) circles. The LRIS field size is $\sim 5\farcm5 \times 7'$, which corresponds to comoving $\sim 7 \times 10\,h^{-1}$ Mpc. The region bounded in black is the area covered by the three slit masks used on this field. [*See the electronic edition of the Journal for a color version of this figure.*]

view of the LRIS camera. In fact, this is true for all fields imaged with the LRIS camera. Figure 11 presents an *R*-band image of the PSS 0808+5215 field. The QSO and spectroscopically confirmed $z > 2$ LBGs are marked in the image; the LBGs near the $z = 2.936$ and 3.114 DLA are indicated separately. The DLA at $z = 2.936$ appears to reside toward the apparent edge of the overdensity. This is an excellent argument for the acquisition of wide-field images in future surveys and is one of the main objectives of our ODD survey. Clustering analysis on scales much larger than the correlation length is necessary for the proper correlation analysis and study of large-scale behavior of LBGs and DLAs.

To test how this overdensity affected the overall DLA-LBG clustering amplitude, we computed the strength of the cross-correlation in the absence of the $z = 2.936$ DLA. We found best-fit values and 1 σ errors of $r_0 = 2.98 \pm 1.34$ and $\gamma = 1.32 \pm 0.34$ using the conventional binning technique, and $r_0 = 2.72^{+1.8}_{-2.1}$ and $\gamma = 1.48^{+1.5}_{-1.1}$ using the maximum likelihood method. The survival of the clustering signal after the omission of the $z = 2.936$ DLA in the PSS 0808+5215 field is further evidence for an overdensity of LBGs near DLAs, on average. In fact, from every measurement and test in this work, a nonzero clustering signal has been detected.

TABLE 3
LBG AUTOCORRELATION PARAMETER SUMMARY

Method	r_0	γ
Conventional Binning[a,b]	2.65 ± 0.5	1.55 ± 0.4
Maximum Likelihood[b]	$2.91^{+1.0}_{-1.0}$	$1.21^{+0.6}_{-0.3}$
Tests		
Conventional Binning[a,c]	2.31 ± 0.6	1.47 ± 0.4
Maximum Likelihood[c]	$2.08^{+1.0}_{-1.1}$	$1.49^{+1.1}_{-0.5}$

[a] Galaxy separations determined using a cylindrical approach described in Appendix C of A03.
[b] Angular positions of galaxies in the random catalogs are identical to the angular positions of the data.
[c] Angular positions of galaxies in the random catalogs are random.

7. GALAXY BIAS AND MASS

The primary objective of this survey was to measure the DLA-LBG cross-correlation function to estimate the DLA galaxy bias in the context of CDM cosmology and use this information to infer the average halo mass of DLAs. This provides a first step in establishing the fundamental properties of the population of protogalaxies that DLAs represent. We were successful in making an independent measurement of the LBG autocorrelation function at $z \sim 3$ and used this as an important calibrator to measure the DLA-LBG cross-correlation function. Although the uncertainties in this work make a direct measure of the DLA bias difficult, it can be estimated in the following way. The relationship between the LBG autocorrelation function $\xi_{\rm LBG}$ and dark matter correlation function $\xi_{\rm DM}$ on scales where the linear bias is a good model is

$$\xi_{\rm LBG}(r) = b^2_{\rm LBG}\xi_{\rm DM}(r), \tag{24}$$

where $b_{\rm LBG}$ is the LBG galaxy bias. Similarly, for the DLA-LBG cross-correlation function, the relationship is (Gawiser et al. 2001)

$$\xi_{\rm DLA\text{-}LBG}(r) = b_{\rm DLA}b_{\rm LBG}\xi_{\rm DM}(r), \tag{25}$$

where $b_{\rm DLA}$ is the DLA galaxy bias. Therefore, the ratio of the two relationships becomes

$$\frac{\xi_{\rm DLA\text{-}LBG}(r)}{\xi_{\rm LBG}(r)} = \frac{b_{\rm DLA}}{b_{\rm LBG}}. \tag{26}$$

Assuming, as we have throughout this paper, that $\xi(r)$ is well fit by a power law of the form $\xi(r) = (r/r_0)^{-\gamma}$, and assuming identical values of γ for both the autocorrelation and cross-correlation functions, this ratio becomes

$$\left(\frac{r_{0,\rm LBG}}{r_{0,\rm DLA\text{-}LBG}}\right)^{-\gamma} = \frac{b_{\rm DLA}}{b_{\rm LBG}} \tag{27}$$

and illustrates that the ratio of the correlation lengths is a direct indicator of the ratio of the biases. These assumptions are reasonable, especially when considering that both r_0 and γ were freely varied when fitting the LBG autocorrelation and DLA-LBG cross-correlation functions using each technique and produced consistent values within their uncertainties (Tables 3 and 4). Moreover, we measured the best-fit values of r_0 for each correlation function at various values of fixed γ and found all resulting correlation lengths to be in agreement within error as well. Table 5 displays the best-fit values for a fixed value of $\gamma = 1.6$.

TABLE 4
DLA-LBG Cross-Correlation Parameter Summary

Method	11 DLAs[a]		15 DLAs[b]	
	r_0	γ	r_0	γ
Conventional Binning[c,d]	3.32 ± 1.3	1.74 ± 0.4	2.20 ± 1.0	1.77 ± 0.4
Maximum Likelihood[d]	$2.81^{+1.4}_{-2.0}$	$2.11^{+1.3}_{-1.4}$	$2.66^{+1.9}_{-2.1}$	$1.59^{+1.6}_{-0.9}$
Tests				
Conventional Binning[c,e]	3.21 ± 1.0	2.03 ± 0.2	2.52 ± 0.9	1.71 ± 0.5
Maximum Likelihood[e]	$3.20^{+2.2}_{-2.9}$	$1.62^{+1.4}_{-1.0}$	$2.44^{+1.3}_{-1.9}$	$2.41^{+1.6}_{-1.7}$

[a] Results using the 11 DLAs from this work.
[b] Results from this work combined with the DLA and LBG information for the four DLAs in the survey of S03.
[c] Galaxy separations determined using a cylindrical approach described in Appendix C of A03.
[d] Angular positions of galaxies in the random catalogs are identical to the angular positions of the data.
[e] Angular positions of galaxies in the random catalogs are random.

It is true that the DLA-LBG cross-correlation function measurement from each method individually can only confirm a nonzero DLA galaxy bias with $\sim$1–2 σ confidence. But the implications from the combined set of measurements and tests of those measurements are what drive our overall claim that DLAs and LBGs likely have similar spatial distributions and galaxy biases. The results indicate not only an overdensity of LBGs near DLAs over random, but also correlation functions of similar form and strength. We find that the average correlation lengths and uncertainties for fixed and varied values of γ for the LBGs in this work correspond to an average $z \sim 3$ LBG galaxy bias between $2 < b_{\rm LBG} < 3$ and $1.5 < b_{\rm LBG} < 3$, respectively. Similarly, the average $z \sim 3$ DLA galaxy bias ranges between $1.3 < b_{\rm DLA} < 4$ and $1.5 < b_{\rm DLA} < 4$ for the 11 DLAs in this survey, and between $1.3 < b_{\rm DLA} < 3$ and $0.8 < b_{\rm DLA} < 3$ for the combined set of 15 DLAs. The average halo mass of a galaxy population can be inferred from the galaxy bias using halo mass function approximations (e.g., Mo et al. 1998; Sheth et al. 2001). The above galaxy bias values correspond to LBG mass ranges of approximately $10^{10.8} < \langle M_{\rm LBG} \rangle < 10^{11.6}$ and $10^{9.7} < \langle M_{\rm LBG} \rangle < 10^{11.6}\ M_\odot$, respectively. The average measurements for the 11 DLAs in this survey lead to approximate mass ranges of $10^9 < \langle M_{\rm LBG} \rangle < 10^{11.9}$ and $10^{9.7} < \langle M_{\rm LBG} \rangle < 10^{12}\ M_\odot$ and approximate mass ranges for the combined set of 15 DLAs of $10^9 < \langle M_{\rm LBG} \rangle < 10^{11.6}$ and $10^{7.3} < \langle M_{\rm LBG} \rangle < 10^{11.7}\ M_\odot$, for fixed and varied values of γ, respectively, in each case. Both the galaxy bias and mass calculations were determined by the method outlined in Quadri et al. (2006).

TABLE 5
Correlation Lengths for $\gamma = 1.6$

Method	LBG-LBG	DLA-LBG (11)[a]	DLA-LBG (15)[b]
Conventional Binning[c,d]	2.72 ± 0.5	3.53 ± 1.0	2.27 ± 1.0
Maximum Likelihood[d]	$3.32^{+0.6}_{-0.6}$	$2.93^{+1.4}_{-1.5}$	$2.66^{+1.2}_{-1.3}$
Tests			
Conventional Binning[c,e]	2.40 ± 0.5	3.87 ± 1.0	2.53 ± 0.8
Maximum Likelihood[e]	$2.96^{+0.6}_{-0.7}$	$3.20^{+1.5}_{-1.7}$	$2.61^{+1.3}_{-1.5}$

[a] Results using the 11 DLAs from this work.
[b] Results from this work combined with the DLA and LBG information for the four DLAs in the survey of S03.
[c] Galaxy separations determined using a cylindrical approach described in Appendix C of A03.
[d] Angular positions of galaxies in the random catalogs are identical to the angular positions of the data.
[e] Angular positions of galaxies in the random catalogs are random.

The $z \sim 3$ LBG correlation length computed by A03 is 3.96 ± 0.29 for the $\mathcal{R} < 25.5$ spectroscopic sample results in an LBG galaxy bias of $b_{\rm LBG} \sim 4$ and corresponds to an average halo mass of $\langle M_{\rm LBG} \rangle \sim 10^{11.9}\ M_\odot$. In addition, it has been shown that the LBG correlation length is dependent on the observed $\mathcal{R}$-band (rest-frame $\sim$1700 Å) luminosity. Giavalisco & Dickinson (2001) found average $z \sim 3$ LBG masses of $\langle M_{\rm LBG} \rangle \sim 10^{12.4}$, 10^{12}, and $10^{11.6}\ M_\odot$ for LBGs with luminosities of $\mathcal{R} = 23$, 25.5, and $\mathcal{R}_{\rm equiv} = 27.0$, respectively, from ground-based and space-based images (see also Foucaud et al. 2003; Adelberger et al. 2005). Similarly, at $z \sim 4$, Kashikawa et al. (2006) found estimated halo masses of $\langle M_{\rm LBG} \rangle \sim 10^{11.7}$–$10^{12}\ M_\odot$ for $23.5 < i' < 25.5$ LBGs, $\langle M_{\rm LBG} \rangle \sim 10^{11.5}$–$10^{11.7} M_\odot$ for $25.5 < i' < 26.5$ LBGs, and $\langle M_{\rm LBG} \rangle \sim 10^{11.3}$–$10^{11.5}\ M_\odot$ for $26.5 < i' < 27.4$ LBGs. From these relationships, it can be assumed that the typical mass of LBGs is below that of the $\mathcal{R} < 25.5$ (and $R < 25.5$) spectroscopic sample.

8. DISCUSSION

In addition to the agreement between the clustering behavior and implied masses of DLAs and LBGs from this work, there appears to be mounting evidence in favor of the idea that high-redshift DLAs and LBGs sample the same population (e.g., Schaye 2001), such as:

1. The two-dimensional $z \sim 3$ DLA-LBG cross-correlation analysis of Bouché & Lowenthal (2004) of two DLAs and one sub-DLA in wide-field images found a nonzero clustering amplitude to more than 2 σ, using a profile similar to the LBG auto-correlation function and sampling the behavior of DLAs with LBGs on angular scales equal to and beyond those in this work ($\sim$1–15 h^{-1} Mpc).
2. Two $z > 2$ DLAs detected in emission and examined in *Hubble Space Telescope* (*HST*) images exhibit properties consistent with those of the LBG population (Møller et al. 2002).
3. The $z \sim 3$ DLA heating rates implied by the C II* method (Wolfe et al. 2003) require localized nearby sources of star formation that are consistent with those found for average LBGs.
4. The Lyα emission of a $z = 2.04$ DLA detected in the trough of the Lyα absorption feature in the spectrum of PKS 0458-02 (Møller et al. 2004) is consistent with LBG Lyα emission.
5. The dearth of faint, high-redshift sources having low in situ star formation rates that meet the criteria required by DLA statistics (Wolfe & Chen 2006) in the *HST* UDF images.
6. The DLA-LBG correlation length of $r_0 \lesssim 2.85\ h^{-1}$ Mpc determined by the hydrodynamic simulations of Bouché et al.

(2005) is in very good agreement with the results from this work and is consistent with the LBG population as a whole.

7. The results from high-resolution numerical simulations of Nagamine et al. (2004a, 2004b, 2006) indicate that strong galactic-scale winds from starbursts evacuate the gas in lower mass ($\langle M_{\rm DLA}\rangle \lesssim 10^8\ M_\odot$) DLAs, driving up the mean DLA mass in the stronger galactic-wind scenarios to values in good agreement with this work and average LBGs.

8. The typical LBG magnitude of $R \sim 27$ and the small impact parameter of $<1''$ is consistent with the very few detections of DLA emission in the sight lines to QSOs.

One picture that could reconcile the above results is where LBGs are starbursting regions embedded in relatively massive DLA systems. The LBG starbursts can provide the necessary heating to explain the observed C II* observations under reasonable geometric assumptions. Although the signal-to-noise ratio of the low-resolution spectra of individual LBGs is poor, the Lyα features that are observed in a subset of LBG spectra appear to be damped. This includes the high signal-to-noise ratio exception of the gravitationally lensed LBG MS 1512-cB58 (Pettini et al. 2002). The dynamics of large systems are able to explain the observed DLA gas kinematics as shown in Prochaska & Wolfe (1997, 1998) and Wolfe & Prochaska (2000a, 2000b). The large radial distribution of cold gas necessary in the semianalytical models of Maller et al. (2001) supports this picture; however, large systems with these properties at high redshift are sometimes difficult to rectify in popular models. In addition, the average metallicity of LBGs ($Z/Z_\odot \sim 1/4$) is typically higher than that of DLAs ($Z/Z_\odot \sim 1/30$), yet the lowest LBG metallicities and highest DLA metallicities overlap. Any perceived discrepancy is likely to be resolved by invoking metallicity gradients and applying feedback, dust, and multiphase arguments, such as those proposed in Nagamine et al. (2004b), to future simulations. What is needed observationally are ground-based surveys focused on the spatial distribution of DLAs and LBGs, in addition to space-based and AO observations revealing the luminosity function and morphologies of DLAs.

9. SUMMARY

Our survey for galaxies associated with DLAs at $z \sim 3$ has been successful in developing an efficient $u'BVRI$ photometric selection technique and color criteria to detect LBGs in QSO fields with known DLAs. We used 211 $z > 2$ LBG spectra to make an independent measurement of the three-dimensional LBG autocorrelation function and the first measurement of the three-dimensional DLA-LBG cross-correlation function.

We used a modified version of the conventional binning technique following the prescription in A03 and measured best-fit values and 1 σ uncertainties of $r_0 = 2.65 \pm 0.48$ and $\gamma = 1.55 \pm 0.40$ for the $z \sim 3$ LBG autocorrelation function. These results are in agreement with the previous measurement by A03 when considering that the uncertainties may be underestimated by a factor of 1–2 (§ 6.1). Applying this technique to the DLA-LBG cross-correlation resulted in best-fit values and 1 σ errors of $r_0 = 3.32 \pm 1.25$ and $\gamma = 1.74 \pm 0.36$ for the set of 11 DLAs in our survey, and $r_0 = 2.20 \pm 0.96$ and $\gamma = 1.73 \pm 0.39$ for the combined set of 15 DLAs that include 4 DLAs from the survey of S03. These results are shown as large diamonds in Figure 12.

Although the above binning technique can produce accurate results, conventional binning techniques in general are dependent on bin size, interval, and bin center. To get around these dependencies, we independently measured the correlation functions using a maximum likelihood technique based on Poisson statistics. This

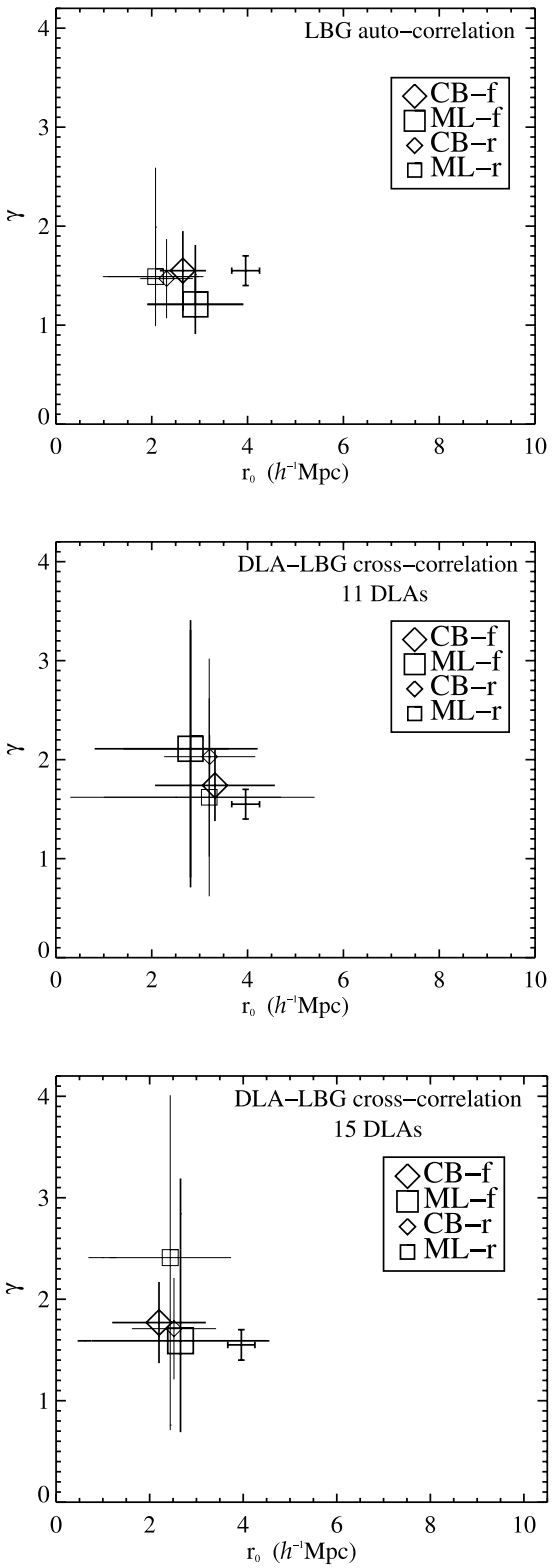


FIG. 12.—Result summary plots for the LBG autocorrelation and DLA-LBG cross-correlation functions. The best-fit values and 1 σ uncertainties are shown for the LBG autocorrelation (*top*), the DLA-LBG cross-correlation for the 11 DLAs in this survey (*middle*), and the full set of 15 DLAs (*bottom*) that includes 4 DLAs from the available data set of S03. Large bold symbols indicate the results for the correlation function measurements, and small symbols indicate the results for the tests on these measurements. The values for the LBG autocorrelation determined by A03 are shown by the error cross at $r_0 = 3.96$, $\gamma = 1.55$ for comparison. The legend code is as follows: CB = conventional binning, ML = maximum likelihood, f = galaxies in the random catalogs having the fixed angular positions of the data, r = galaxies in the random catalogs having random positions. [*See the electronic edition of the Journal for a color version of this figure.*]

method is bin-independent, makes full use of the data, and is ideal for small data sets. We found maximum likelihood values and 1 σ confidence levels of $r_0 = 2.91^{+1.0}_{-1.0}$, $\gamma = 1.21^{+0.6}_{-0.3}$ for the LBG autocorrelation function, and $r_0 = 2.81^{+1.4}_{-2.0}$, $\gamma = 2.11^{+1.3}_{-1.4}$ and $r_0 = 2.66^{+1.9}_{-2.1}$, $\gamma = 1.59^{+1.6}_{-0.9}$ for the DLA-LBG cross-correlation functions for the sets of 11 and 15 DLAs, respectively. The results for both the autocorrelation and the cross-correlation are indicated by large squares in Figure 12.

We tested the effects that the physical constraints of the slit masks have on the angular component of the correlation function by reanalyzing the data by means of the above two techniques and assigning random angular positions to the random galaxy catalogs instead of the angular positions of the data, as was imposed in the original analysis. The test results using the conventional binning technique are shown as small diamonds in Figure 12 and as small squares using the maximum likelihood technique.

Furthermore, we discovered a relative spike of five LBGs within $\Delta z = 0.015$ of the $z = 2.936$ DLA in the field PSS 0808+5215 and tested the average DLA-LBG clustering signal in the absence of this DLA. As expected, the amplitude of the clustering was diminished, but the overdensity and form of the correlation function survives and remains in good agreement with the values determined for the complete set of DLAs.

Finally, we found that two of the six QSOs in the survey spectra lie within $\Delta z = 0.0125$ of two of the DLAs. We determine a 1 in 940 chance of this occurring randomly and interpret this to suggest a possible relationship between the distribution of QSOs and DLAs at $z \sim 3$. If found to be a common occurrence, the close proximity of QSOs to DLAs could lend insight into the duty cycle of QSOs and the size and persistence of systems with high H I column densities near sources of significant ionizing radiation.

It can be seen from Figure 12 that all of the independent methods varying both r_0 and γ, and tests of those methods, produce results that are in agreement within their uncertainties. This is also true for the measurements of r_0 holding γ fixed when using all methods (Table 5). The DLA-LBG cross-correlation function, determined from both the set of 11 DLAs in our survey and the combined set of 15 DLAs, exhibits a measurable clustering signal and has best-fit parameters in agreement with those of the LBG autocorrelation function. The individual measurements of the DLA-LBG cross-correlation function are only able to measure the DLA galaxy bias to 1–2 σ, and we expect to improve this measurement to $\sim 3\,\sigma$ significance when combining these results with those of our ODD survey in progress. When letting r_0 and γ vary, we found that the best-fit values and their uncertainties suggest an LBG galaxy bias of $1.5 < b_{\rm LBG} < 3$, corresponding to an average halo mass of $10^{9.7} < \langle M_{\rm LBG} \rangle < 10^{11.6}\ M_\odot$. The DLA galaxy bias determined identically for the 11 DLAs in this survey is $1.3 < b_{\rm DLA} < 4$ and infers an average DLA mass of $10^{9.7} < \langle M_{\rm LBG} \rangle < 10^{12}\ M_\odot$. These values are $0.8 < b_{\rm DLA} < 4$ and $10^{7.3} < \langle M_{\rm LBG} \rangle < 10^{11.7}\ M_\odot$ for the combined set of 15 DLAs. Finally, we offer the plausible scenario that LBGs reside in the same systems that host DLAs. We identify several pieces of evidence in the literature that support this view. Whatever the true picture, the results from this survey have shed light on the elusive mass of DLAs, their distribution with LBGs, and a possible link between the distribution of QSOs and DLAs at $z \sim 3$.

The authors wish to thank C. Mullis and K. L. Adelberger for very helpful discussions. In addition, we would like to thank A. Dressler, R. Giovanelli, and J. Darling for access to the Palomar Observatory and for observational assistance with the COSMIC camera. The authors recognize and acknowledge the very significant cultural role and reverence that the summit of Mauna Kea has always had within the indigenous Hawaiian community. We are most fortunate to have the opportunity to conduct observations from this mountain. This work was partially supported by the National Science Foundation grant AST 03-07824 and the NSF Astronomy and Astrophysics Postdoctoral Fellowship (AAPF) grant AST 02-01667 awarded to Eric Gawiser.

REFERENCES

Adelberger, K. L. 2005, ApJ, 621, 574
Adelberger, K. L., Steidel, C. C., Giavalisco, M., Dickinson, M., Pettini, M., & Kellogg, M. 1998, ApJ, 505, 18
Adelberger, K. L., Steidel, C. C., Pettini, M., Shapley, A. E., Reddy, N. A., & Erb, D. K. 2005, ApJ, 619, 697
Adelberger, K. L., Steidel, C. C., Shapley, A. E., & Pettini, M. 2003, ApJ, 584, 45 (A03)
Bouché, N., Gardner, J. P., Katz, N., Weinberg, D. H., Davé, R., & Lowenthal, J. D. 2005, ApJ, 628, 89
Bouché, N., & Lowenthal, J. D. 2004, ApJ, 609, 513
Cooke, J., Wolfe, A. M., Gawiser, E., & Prochaska, J. X. 2006, ApJ, 636, L9
Cooke, J., Wolfe, A. M., Prochaska, J. X., & Gawiser, E. 2005, ApJ, 621, 596 (Paper I)
Croft, R. A. C., Dalton, G. B., Efstathiou, G., Sutherland, W. J., & Maddox, S. J. 1997, MNRAS, 291, 305
Daddi, E., Cimatti, A., Pozzetti, L., Hoekstra, H., Rottgering, H. J. A., Renzini, A., Zamorani, G., & Mannucci, F. 2000, A&A, 361, 535
Daddi, E., et al. 2004, ApJ, 600, L127
Davis, M., & Peebles, P. J. E. 1983, ApJ, 267, 465
Foucaud, S., McCracken, H. J., Le Fèvre, O., Arnouts, S., Brodwin, M., Lilly, S. J., Crampton, D., & Mellier, Y. 2003, A&A, 409, 835
Gawiser, E., Wolfe, A. M., Prochaska, J. X., Lanzetta, K. M., Yahata, N., & Quirrenbach, A. 2001, ApJ, 562, 628
Giavalisco, M., & Dickinson, M. 2001, ApJ, 550, 177
Hawkins, E., et al. 2003, MNRAS, 346, 78
Kashikawa, N., et al. 2006, ApJ, 637, 631
Kauffmann, G. 1996, MNRAS, 281, 475
Kells, W., Dressler, A., Sivaramakrishnan, A., Carr, D., Koch, E., Epps, H., Hilyard, D., & Pardeilhan, G. 1998, PASP, 110, 1487
Kerscher, M., Szapudi, I., & Szalay, A. S. 2000, ApJ, 535, 13
Landy, S. D., & Szalay, A. S. 1993, ApJ, 412, 64
Lowenthal, J. D., et al. 1997, ApJ, 481, 673
Lu, L., Sargent, W. L. W., & Barlow, T. A. 1998, AJ, 115, 55
Maller, A. H., Prochaska, J. X., Somerville, R. S., & Primack, J. R. 2001, MNRAS, 326, 1475
McCarthy, P. J., et al. 2001, ApJ, 560, L131
———. 2004, ApJ, 614, 9
Mo, H. J., Mao, S., & White, S. D. M. 1998, MNRAS, 295, 319
Møller, P., Fynbo, J. P. U., & Fall, S. M. 2004, A&A, 422, L33
Møller, P., Warren, S. J., Fall, S. M., Fynbo, J. P. U., & Jakobsen, P. 2002, ApJ, 574, 51
Mullis, C. R., Henry, J. P., Gioia, I. M., Böhringer, H., Briel, U. G., Voges, W., & Huchra, J. P. 2004, ApJ, 617, 192
Nagamine, K., Springel, V., & Hernquist, L. 2004a, MNRAS, 348, 421
———. 2004b, MNRAS, 348, 435
Nagamine, K., Wolfe, A. M., Springel, V., & Hernquist, L. 2006, MNRAS, submitted
Oke, J. B., et al. 1995, PASP, 107, 375
Peebles, P. J. E. 1980, The Large-scale Structure of the Universe (Princeton: Princeton Univ. Press)
Péroux, C., Storrie-Lombardi, L. J., McMahon, R. G., Irwin, M., & Hook, I. M. 2001, AJ, 121, 1799
Pettini, M., Rix, S. A., Steidel, C. C., Adelberger, K. L., Hunt, M. P., & Shapley, A. E. 2002, ApJ, 569, 742
Pettini, M., Shapley, A. E., Steidel, C. C., Cuby, J.-G., Dickinson, M., Moorwood, A. F. M., Adelberger, K. L., & Giavalisco, M. 2001, ApJ, 554, 981
Pettini, M., Steidel, C. C., Adelberger, K. L., Dickinson, M., & Giavalisco, M. 2000, ApJ, 528, 96
Porciani, C., & Giavalisco, M. 2002, ApJ, 565, 24
Press, W. H., Flannery, B. P., Teukolsky, S. A., & Vetterling, W. T. 1992, Numerical Recipes in C (Cambridge: Cambridge Univ. Press)

Prochaska, J. X., Gawiser, E., Wolfe, A. M., Cooke, J., & Gelino, D. 2003, ApJS, 147, 227
Prochaska, J. X., Herbert-Forte, S., & Wolfe, A. M. 2005, ApJ, 635, 123
Prochaska, J. X., & Wolfe, A. M. 1997, ApJ, 487, 73
———. 1998, ApJ, 507, 113
Prochaska, J. X., et al. 2001, ApJS, 137, 21
Quadri, R., et al. 2006, ApJ, in press (astro-ph/0606330)
Roche, N., Eales, S. A., Hippelein, H., & Willott, C. J. 1999, MNRAS, 306, 538
Schaye, J. 2001, ApJ, 559, L1
Schneider, D. P., Schmidt, M., & Gunn, J. E. 1991, AJ, 101, 2004
Shapley, A. E., Steidel, C. C., Adelberger, K. L., & Pettini, M. 2003, ApJ, 588, 65
Sheth, R. K., Mo, H. J., & Tormen, G. 2001, MNRAS, 323, 1
Steidel, C. C., Adelberger, K. L., Dickinson, M., Giavalisco, M., Pettini, M., & Kellogg, M. 1998, ApJ, 492, 428
Steidel, C. C., Adelberger, K. L., Shapley, A. E., Pettini, M., Dickinson, M., & Giavalisco, M. 2003, ApJ, 592, 728
Steidel, C. C., Giavalisco, M., Dickinson, M., & Adelberger, K. L. 1996a, AJ, 112, 352
Steidel, C. C., Giavalisco, M., Pettini, M., Dickinson, M., & Adelberger, K. L. 1996b, ApJ, 462, L17
Storrie-Lombardi, L., & Wolfe, A. M. 2000, ApJ, 543, 552
Wolfe, A. M. & Chen, H.-W. 2006, ApJ, 652, 981
Wolfe, A. M., Gawiser, E., & Prochaska, J. X. 2005, ARA&A, 43, 861
Wolfe, A. M., Lanzetta, K. M., Foltz, C. B., & Chaffee, F. H. 1995, ApJ, 454, 698
Wolfe, A. M., & Prochaska, J. X. 2000a, ApJ, 545, 591
———. 2000b, ApJ, 545, 603
Wolfe, A. M., Prochaska, J. X., & Gawiser, E. 2003, ApJ, 593, 215
Wolfe, A. M., Turnshek, D. A., Smith, H. E., & Cohen, R. D. 1986, ApJS, 61, 249